Construction and Building Materials 173 (2018) 550–572

Contents lists available at ScienceDirect

Construction and Building Materials

journal homepage: www.elsevier.com/locate/conbuildmat

# Evaluation of blast resistance and failure behavior of prestressed concrete under blast loading

Ji-Hun Choi [a], Seung-Jai Choi [a], Jang-Ho Jay Kim [a,*], Ki-Nam Hong [b]

[a] Concrete Structural Engineering Laboratory, School of Civil and Environmental Engineering, Yonsei University, 50 Yonsei-Ro, Seodaemun-Gu, Seoul 03722, Republic of Korea
[b] Concrete Structural Engineering Laboratory, School of Civil Engineering, Chungbuk National University, San 12 Gaesin-dong, Cheongju-si, Chungbuk-do 361-763, Republic of Korea

## HIGHLIGHTS

- The blast resistant capacities of unbounded bi-directional PSC are experimentally and numerically evaluated.
- The blast test procedure and measurement system are established and used to determine blast resistance capacity.
- The simulation model of prestressed concrete panel under blast loading is calibrated using the test data.
- The PSRC members had significantly better blast resistance than RC and PSC members.

## ARTICLE INFO

*Article history:*
Received 20 September 2017
Received in revised form 5 April 2018
Accepted 6 April 2018
Available online 24 April 2018

*Keywords:*
Extreme loading
Bi-directional PSC
Blast resistance
Protective capacity
Blast load

## ABSTRACT

In recent years, frequent terror and military attack by explosion and impact have occurred all over the world. Particularly, World Trade Center collapse and US Department of Defense Pentagon attack on Sept. 11 of 2001 and Fukushima nuclear power plant accident due to Northeast earthquake tsunami on the coast of Japan on Mar. 11 of 2011 resulted in devastating human casualties and structural collapses. These terrors and accidents raised public concerns and anxiety of potential structural collapse of major infrastructures and structures. In order to better combat these problems, the extreme loading resistant structural studies are initiated. Among numerous types of target structures, one of the most important structural types is prestressed concrete (PSC), which is widely used for construction of nuclear containment vessel and gas storage tank. In this study, to evaluate the blast resistance and protective capacity of bi-directional PSC member, blast tests were carried out on 1400 × 1000 × 300 mm reinforced concrete (RC), prestressed concrete without rebar (PSC), prestressed concrete with rebar (PSRC) specimens. The applied blast load was generated by detonating 25 kg ANFO explosive charge at 1.0 m standoff distance. The data acquisitions included blast waves of incident pressure, reflected pressure, and impulse as well as behavioral displacements of deflection, acceleration, and strains of concrete, rebar, and PS tendon. Then, the blast test results are used to calibrate finite element simulation model. Once the simulation model is calibrated, it is used to perform parametric study on bi-directional prestressed concrete specimens to further evaluate the blast resistance of the panels. The study results are discussed in detail in the paper.



## 1. Introduction

### 1.1. Background

In recent years, explosions, collisions, and fires have occurred frequently around the world due to terror attacks and impact accidents. Particularly, since the 9.11 terror attacks on the World Trade Center and the Pentagon of the USA in 2001, public anxiety heightened due to lack of safety in our society. According to data published by the National Intelligence Service of Korea in 2009, 55.2% of terror incidents are related to infrastructures, which led to property damages and human casualties [1]. Especially, since the Korea peninsula is the only divided area in the world with unceasing military confrontations, South Korea has suffered various provocative aggressions from North Korea by means of infiltration, terror, provocations, and bombings for the past 63 years after the Armistice Agreement. Since the sinking of Cheonan Battleship of South Korea by the torpedo and cannon attacks of North Korea near the Coast of Yeonpyeong Island in 2010, public concerns of bombing and terror attacks have continuously increased. The aforementioned incidents can be viewed as representative

* Corresponding author.
*E-mail address:* jjhkim@yonsei.ac.kr (J.-H.J Kim).

https://doi.org/10.1016/j.conbuildmat.2018.04.047
0950-0618/

examples of possible extreme loading scenarios that can occur for structures and infrastructures. Among all of structures and infrastructures, prestressed concrete containment vessels (PCCVs) and liquefied natural gas (LNG) storage tanks are the most vulnerable structures from terrors and accidents. For example, the public fear of nuclear accidents from nuclear containment vessel damages, which have great physical and environmental consequences, drastically increased since the Fukushima Daiichi nuclear disaster in 2011.

Generally, PCCVs and LNG storage tanks are constructed as bi-directional prestressed concrete (PSC) shell structure. Because of the vulnerability of these containment structures under extreme loading scenarios, various studies on physical and structural safety of PSC structures from extreme loading conditions have been conducted by researchers all over the world [2–10]. However, due to national security reasons, only minute number of blast experimental results on structural blasting have been disclosed or published in the past. Because of lack of published study results, no clear standards or specifications in the form of design codes of civil structures related to explosion protection and structural resistance design are available presently.

When a high strain rate inducing load such as blast or impact is applied to a PSC member, it is near impossible to capture the high strain rate behavior of the member and to obtain accurate test data. Also, due to expensive experiment cost and limited test site availability of blast or impact test, it is difficult to conduct sufficient number of experiments. Therefore, only feasible way to understand the damage behavior of PSC structural member is to study those using High Fidelity Physic Based (HFPB) simulations. In HFPB simulation, precise and accurate high strain rate representing loading conditions, material constitutive relations, detailed structural information, and boundary conditions must be used. Also, due to the high strain rate induced multiple time increment simulation, an explicit rather than implicit finite element analysis (FEA) must be performed. Most importantly, HFPB FEA simulation program has to be calibrated by the precisely controlled experimental results, or else the simulation results cannot be considered accurate. Therefore, in this study, a model blast test series is carried out by minimizing the variabilities that can exist in blast test, such as loading condition, structural details, material properties, and boundary conditions. The blast experiment is performed on bi-directional PSC member using 25 kg ANFO charge with a stand-off distance of 1.0 m. The PSC specimen used in blast experiment is modeled as a PSC panel representing an outer wall of prestressed concrete containment vessel (PCCV). Also, the test setup is such that the panel is buried in the ground to only have a top surface directly exposed to the blast pressure to eliminate other reflected blast waves from hitting the specimen. Using the state-of-the-art high strain rate measurement system, the blast test results such as maximum and residual deflections, incident and near field blast pressures, high speed camera recorded deflection behavior, crack pattern, prestressing force loss, and specimen acceleration are obtained. The experimental data, such as fracture mode, energy absorption capacity, displacement, prestressing force variation, and acceleration measured from the blasted specimens are used to calibrate HFPB simulation code. After the calibration, the calibrated HFPB FEA simulation programs can be used to simulate and analyze real extreme loading scenarios of real scale PCCVs and LNG storage tanks.

### 1.2. Literature review

Numerous researches on the structural behaviors subjected to blast loads have been actively conducted. Study results on blast loading were conducted by Protective Design Center (PDC) in the US Army Corps of Engineers to develop ConWEP, for the calculating blast pressures from bomb explosions and to develop a simple single degree of freedom simulation program SBEBD for designing of protective structures in the 1990 s. Based on these findings, TM5-1300 technical manual was published to establish basic principles about disaster preventive technology for concrete structures and to implement these technologies in the designs. Under the supervision of the US Nuclear Regulatory Commission (NRC), Sandia National Laboratory of the US constructed a 1/6 and 1/4 scale model of a RC and PSC reactor containment structure, respectively, to experimentally evaluate their behaviors at ultimate load [3].

Ross et al. (1997) evaluated the behavior of beams and slabs under explosive loads, ANFO explosion experiments were carried out to determine the explosion resistance performance of concrete members [11]. Muszynski et al. (2003) experimentally evaluated blast behavior of RC members by applying explosive pressure to different reinforced concrete wall structures [12]. Morrill et al. (2004) examined the feasibility of the analytical method by comparing and analyzing the results of the finite element simulations and the deflection behavior of the concrete columns and walls from the explosion tests [13]. Davison et al. (2004) and Oesterle (2009) have experimentally and analytically evaluated the protective performance of concrete masonry walls such as FRP and Polyurea, respectively [14,15].

In Korea, impact resistance design for ultimate load is only required in high security facilities. Currently, no clear design standards on protection and explosion-proof structures have been established in Korea. However, the present design codes need suitable provisions of new, retrofit, and strengthening systems for protection of structures and infrastructure under extreme loading scenarios. Recently, a number of blast protection and explosion-proofing studies were performed. The studies included the development of fiber concrete application technology for containment buildings considering airplane collision [16,17], the development of repair and strengthening technology for fire and explosion proofing [18–20], and the construction of APR-1400 physical protection design system [9,21,22]. They were conducted to improve the impact- and explosion-proof performance of concrete structures.

Also, many experimental investigations on high speed load in concrete structures have been conducted all over the world. However, few experimental data on major containment structures such as PCCVs and LNG storage tanks have been disclosed due to national security reasons. Therefore, the present study aims to obtain precise data on blast loaded PSC members by conducting a set of explosion test to investigate blast-resistance capacity and damage behavior of nuclear PCCV outer wall.

## 2. Modeling of blast experiments

In order to find a suitable blast loading scenario for a blast incident of nuclear PCCV, a blast scenario of an explosion occurring on a ground level at a short distance away to the target PCCV is considered. In order to model the actual PCCV applied with blast loading, the scale of the target structure and the blast source must be scaled down. Therefore, the theoretical backgrounds of blast induced loading and scaled down structural modeling must be investigated thoroughly.

In this study, a panel specimen representing the wall of a PCCV was fabricated. The thickness of the test specimens is taken as a quarter thickness of the actual thickness. Due to the restriction in dimensions of the test specimens, only feasible thickness was 1/4 thickness. Even though thickness of the specimen was reduced to 1/4 size, the rebar and tendon ratios were kept as same as the actual PCCV wall. Also, the rebar, tendon, and concrete strengths were kept as same as the actual PCCV wall. A report by Construc-

tion Technology Laboratories (CTL), showed that, when the specimen geometrical dimensions are varied while using the same material properties, blast behavior of concrete member remained the same [26,27]. Based on this concept, the panel specimens were design to have dimensions of 1400 × 1000 × 300 mm while rebar, tendon, and concrete strengths as well as rebar and tendon ratios were as same as the actual PCCV wall.

### 2.1. Blast loading scenario

In any blast scenario, wave pressure variations can occur due to the ground reflection and absorption of wave pressure where the absorptions vary depending on the condition of ground surface. Therefore, it is necessary to determine the blast loading scenario to calculate precise wave pressure magnitude and shape depending on a blast weight and a standoff distance. In order to achieve this task, two scenarios were selected. One is a blast occurring from a truck parked in front of a PCCV and the other is a blast occurring from of an aircraft explosion in the air.

Since design criteria of blast loading does not exist for real nuclear power plant structures, postulated pressure waves for Uljin Nuclear Power Plant 1 and 2 is used, which was designed by Flamatome in France as shown in Fig. 1. More precisely, a blast pressure with a speed of 350 m/s and a magnitude of 0.005 MPa for a time duration of 300 ms is selected as loading condition [23]. As shown in Fig. 1, by applying this loading condition, an initial pressure has a minimal impact. However, since the loading time duration of 300 ms is relatively long time duration for blast loading, the pressure magnitude can be calculated using ConWEP program, a conventional weapon induced pressure calculation program described in TM5-855-1 [24].

The Hopkinson-Cranz Scaling Law was used to apply the real blast loading scenario to the experimentally constrained condition. The law implies that when a different amount of the same type of two explosives is blasted in the atmosphere, it creates a highly similar blast wave in the same scale distance. A scale distance presented in Eq. (1) is used as a dimension variable.

$$Z = \frac{R}{E^{1/3}} \quad \text{or} \quad Z = \frac{R}{W^{1/3}} \tag{1}$$

where, $R$ is a distance from the center of the explosive; $E$ is a total blast heat of the explosive; $W$ is a gross weight of standard explosive, such as TNT. Extensive data on blast induced pressure were calculated using the scale law and are presented in TM5-1300 [25]. An equivalent weight of explosive charge is calculated according to the scale law of Eq. (1) in the present study to select the blast

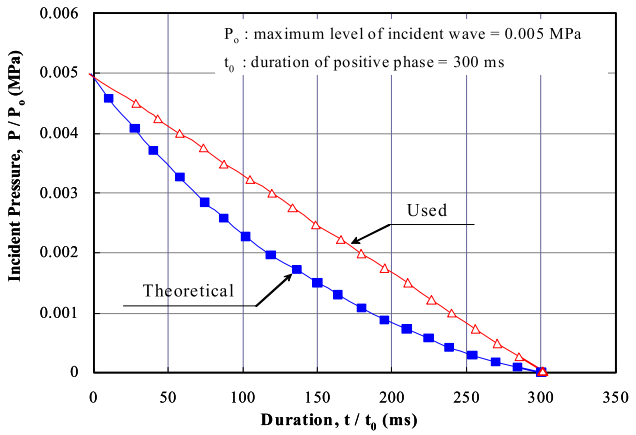


**Fig.1.** Applied incident pressuretime duration curve of the external shock wave on reactor containment structural design criteria [23].

type. Using this blast load, an explosion test was conducted using 25 kg of ammonium nitrate/fuel oil (ANFO) explosive at 1.0 m height above the ground surface. In the past researches, TNT explosives were used. However, due to flying steel casing debris from TNT explosion, the surface of the specimen was heavily damaged and the pressure measuring pressuremeter was knocked out. In order to eliminate the problems associated with TNT explosive, ANFO charge is selected as an explosive for this study [17].

### 2.2. Specimen scaling theory

APR-1400 PCCV, the next generation PCCV for Korean nuclear power plant, is selected as the target structure for the blast test in this study. Since the outer wall of a PCCV is designed and constructed as a bi-directional prestressed concrete (PSC) member, the bi-directional PSC panel is chosen as a specimen type. Based on the PS tendon arrangement in a standard PCCV outer wall as shown in Fig. 2, the tendon arrangement of the APR-1400 is assumed. In a standard PCCV, PS tendon layout is in two directions (vertical and meridional) for the outer wall and three arcs with an angle difference of 120° for the roof dome. The wall has three or four buttress for post-tensioned tendon anchoring [22].

In the outer wall, it is structurally advantageous to place PS tendons inside of the outer reinforcing bars, the vertical tendons to pass through the center of the wall, and the meridional tendons toward outer surface of the wall as far as possible. Based on the basic guidelines described above, the target specimen is modeled to be compatible to the design details. In this study, the specimens are modeled as a scaled down version of the wall and to behave in same manner as the PCCV wall applied with blast pressure. It is important to note that the scaled down model of the actual PCCV has to have similar accelerations and deflections from the blast load as those of the actual PCCV wall. However, it is extremely difficult to model the scaled down specimen just by applying the similitude laws. A published report by Construction Technology Laboratory (CTL) of the United States stated that a common bi-directional PSC outer wall of the PCCV in the US is modeled for a structural test by reducing the thickness to a half of the actual size, while maintaining the other dimensions and material parameters [26,27]. Even though this type of the specimen modeling did not apply similitude scale laws, the test results showed that structural behavior of the specimen closely resembled the results from the full scale PCCV.

In this study, the thickness of the wall is reduced to 1/4 of the actual size scale, while maintaining the other dimensions and material parameters. However, due to the reduction in the thickness, the PS force is scaled down with respect to the thickness ratio. More specifically, thickness of the specimen was 300 mm, which corresponds to 1/4 of the full scale outer wall thickness of 1.2 m of the nuclear reactor PCCV.

When the top surface of the specimen (e.g., the surface directly exposed to the blast charge) is placed at the ground surface level, this blast can be considered as a free explosion occurring in the atmosphere. In order to apply the full wave pressure on the specimen surface, while the explosion occurs in the mid-air at 1.0 m standoff distance away from the loaded surface. The specimen dimensions are selected as 1400 × 1000 × 300 mm. This specimen size receives the explosive pressure load evenly on the top surface with minimum diffraction and interference effect. Reinforcement ratio of 0.024 and the PS tendon ratio of 0.0107 are used, which are same as those used in the full scale outer wall of nuclear PCCVs.

### 2.3. Test setup

In order to measure the structural behavior of the specimen applied with a blast load, a device capable of precisely measuring

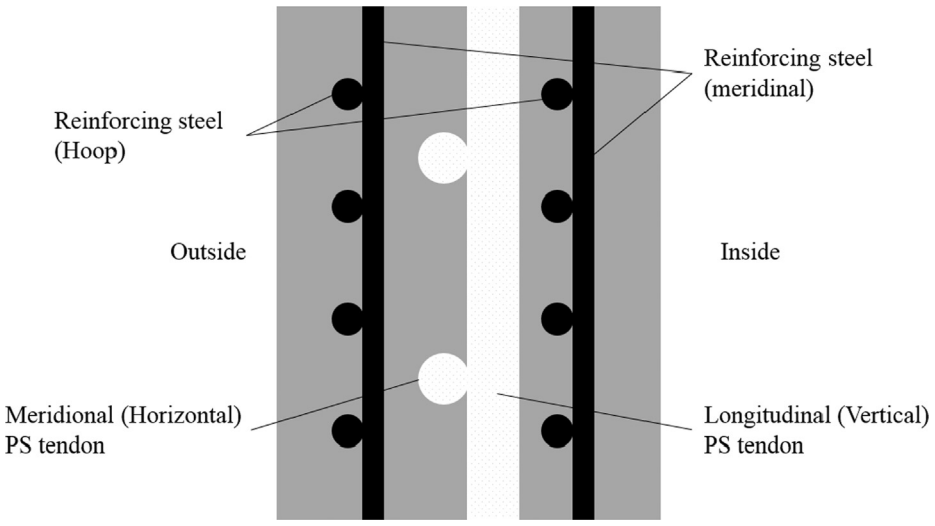


**Fig. 2.** Details of PCCV outer wall [22].

the deformation of the structure is needed. Since a blast load transmits a very strong impulse in short time duration, the measuring device has to capture the motion of the structure at instantaneous time increments. The measurement support frame used for the blast test is shown in Fig. 3. In order to expose the top surface of the specimen on the ground level with a hollow space underneath for data measurements, a steel frame with a thickness of 20 mm was constructed using high-strength steel to be buried in the ground. It is important to note that the frame stiffness must be stiff enough under blast loading to have no rigid body motion throughout the test. When the specimen is mounted on the frame, it is fitted firmly into the L-shaped top frame. Then, the specimen is fixed to the frame by using 8C-clamp on each side of the specimen. The clamps are used to allow rotation on the supports while preventing uplift and vibration of the specimen during blast loading. In order to facilitate the installation of the measurement devices during the blast test, another manhole next to the specimen is constructed as shown in Fig. 3. The opening of the manhole is covered with a thick steel plate during testing. The measurement system procedure used in the study is shown in Fig. 5. The data measuring and capturing devices are all capable of operating at a sampling rate of 500 kHz or higher. As shown in Fig. 4, each measurement sensor receives signal through the Field Receiver Junction box located approximately 200 m away from the test site. Through a signal conditioner composed of a filter and an amplifier, the analog signal is digitized through a Data Acquisition (DAQ) system. Signal processing is performed using in a program such as Labview-based FlexPro 7.0.

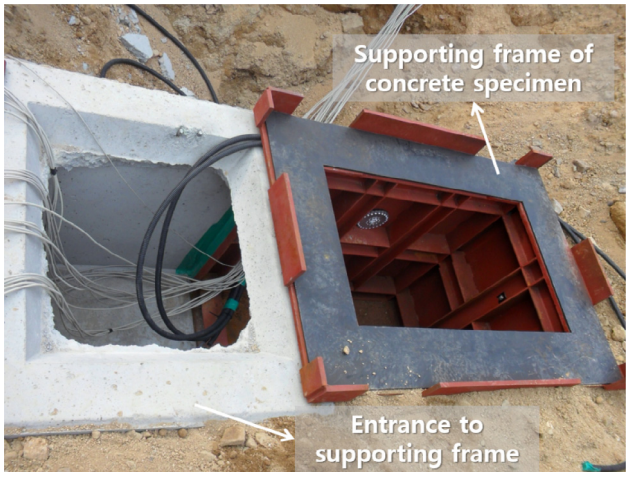


**Fig. 3.** Support frame of panel specimen.

## 3. Blast test details

### 3.1. Test specimen design and fabrication

In order to investigate the blast resistant capacity behavior of the bi-directional PSC panel members for calibration of FEA

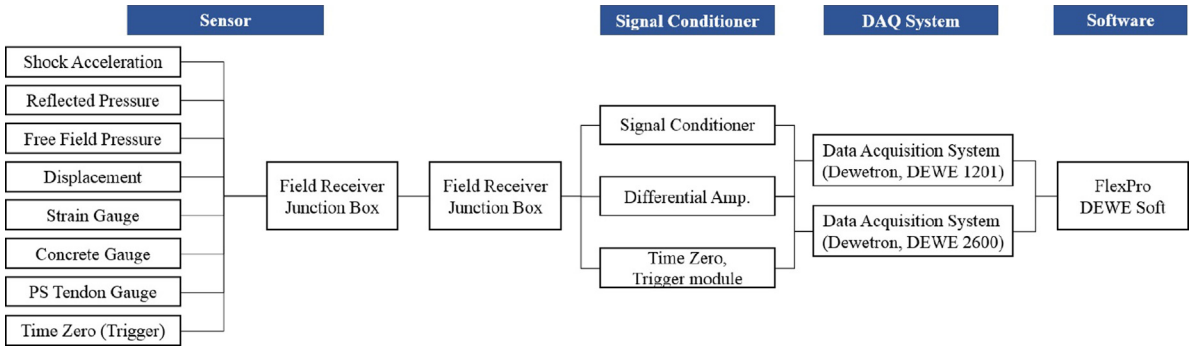


**Fig. 4.** Measurement system details and procedure.

simulation, precise data must be acquired. Due to limited research fund, experimental site, and explosive licensing, a full-scale PCCV blast test was not possible. Therefore, only a scaled-down model test was feasible. The specimen dimensions and details are shown in Fig. 5. Three types of specimens were manufactured: reinforced concrete (RC), prestressed concrete without rebar (PSC), and prestressed concrete with rebar (PSRC). For the RC specimen, D13 rebars with grid orientation were used for top and bottom reinforcements at a constant spacing of 100 mm. PS tendon used in the PSC and PSRC specimens were a 15.2 mm PS mono-strand, which can develop efficient concrete confinement from biaxial stress condition. In order to study the effect of PS force variation on the blast behavior of a biaxial PSC panel, 2 types of steel strand were used. SWPC 7B (type B) is a strand with yield strength of 1600 MPa, ultimate strength of 1730 MPa, and unit weight of 1.101 kg/m, while SWPC 7D (type D) is a strand with yield strength of 2040 MPa, ultimate strength of 2400 MPa, and unit weight of 1.101 kg/m. The material properties of the two strand types are shown in Table 1. Since the tendons used in the actual PCCVs are post-tensioned type. Since the PCCV is an unbonded prestressed concrete, six strands are installed in 80 mm diameter sheath tube. Then, post-tensioning is performed without grouting, making the specimen unbonded prestressed concrete.

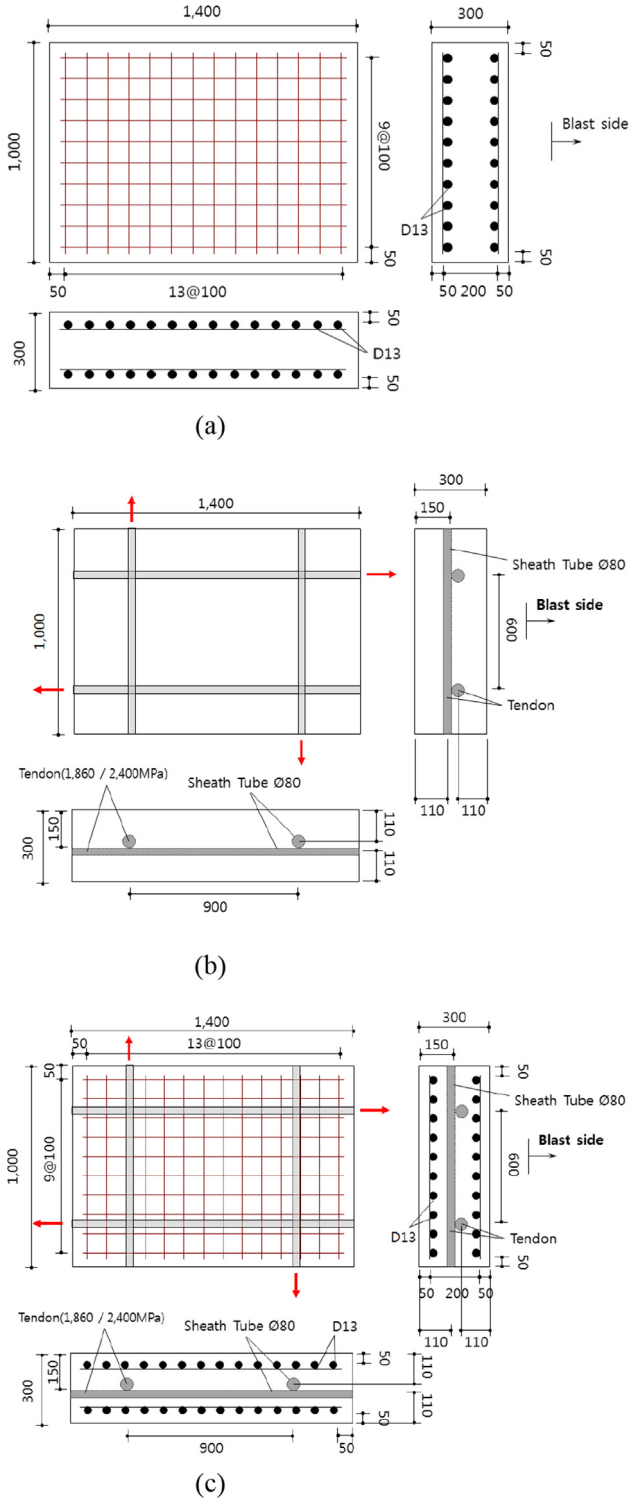


**Fig. 5.** Specimen types and details (unit: mm): (a) RC specimen; (b) PSC specimen; (c) PSRC specimen.

The specimen was cast using concrete with compressive strength of 40 MPa. The mix proportion design of the concrete is shown in Table 2, which is same as the concrete used to cast the actual PCCV. More specifically in the mix design, blast furnace slag powder of 15% to the volume weight of OPC cement was added to develop a target design strength and high performance AE water-reducing admixture was used to improve workability. Bi-directional prestressing forces were applied to the PSC and PSRC specimens after sufficient concrete strength was developed, in order to prevent bearing failure from occurring of the anchorage area during prestressing process. The target prestressing force for B and D type tendon specimens were prestressed with 580 kN and 820 kN, respectively. The actual prestressing force applied to B and D type tendon was 520–610 kN and 690–820 kN, respectively. An accurate PS force was applied to the tendons by measuring the tendon strains during PS process. The tendons were anchored using wedge type anchor heads. The nomenclature used for the specimen titles are explained in Fig. 6.

### 3.2. High strain rate compatible measurement system

The blast test was conducted at Darakdae Test Site of the Agency for Defense Development (ADD) Research Center in Korea. Reflection pressure applied to the concrete specimen was measured at the top surface, 300 mm away from the center of the specimen. The sensors, displacement meter, steel strain gauge, accelerometer, and pressure gauge attached to the specimen are shown in Fig. 7. Rebar strain gauges were attached to the tension part of both ends of rebar, and concrete strain gauge was attached to the center of the upper and lower surfaces of the specimen, at 300 mm away from the center. Free field incident pressure was measured at 5 m away from the specimen, as shown in Fig. 8. As shown in Fig. 9(8), spring type linear variable differential transformer (LVDT) with a displacement capacity of 50 mm was attached at the center of the bottom surface to measure deflection of the specimen behavior. Also, LVDTs were placed on the bottom surface at 250 mm and 350 mm away from the center to measure residual displacements. In order to obtain acceleration data of the

**Table 1**
Material properties of PS strand.

| Properties | Value | |
|---|---|---|
| Type of tendon | SWPC 7B | SWPC 7D |
| Diameter (mm) | 15.2 | 15.2 |
| Cross sectional area (mm$^2$) | 138.7 | 138.7 |
| Unit weight (kg/m) | 1.101 | 1.101 |
| Yield load (kN) | 222 | 283 |
| Ultimate load (kN) | 261 | 333 |
| Yield Strength (MPa) | 1600 | 2040 |
| Tensile Strength (MPa) | 1730 | 2400 |
| Elastic modulus (MPa) | 200,000 | 200,000 |

**Table 2**
Concrete mix proportion design.

| MCA[1] (mm) | Slump (mm) | W/B (%) | S/a (%) | Unit weight (kg/m$^3$) | | | | | |
|---|---|---|---|---|---|---|---|---|---|
| | | | | W | Binder | | S | G | AE |
| | | | | | C | GGBS[2] | | | |
| 25 | 180 | 33.0 | 46.5 | 165 | 425 | 75 | 786 | 918 | 4.0 |

1. MCA: Maximum size of Coarse Aggregate.
2. GGBS: Ground Granulated Blast-furnace Slag.

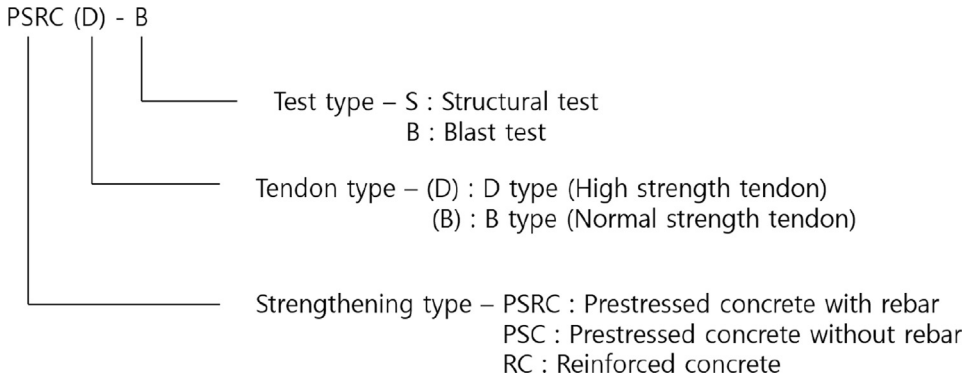


**Fig. 6.** Nomenclature of specimen title.

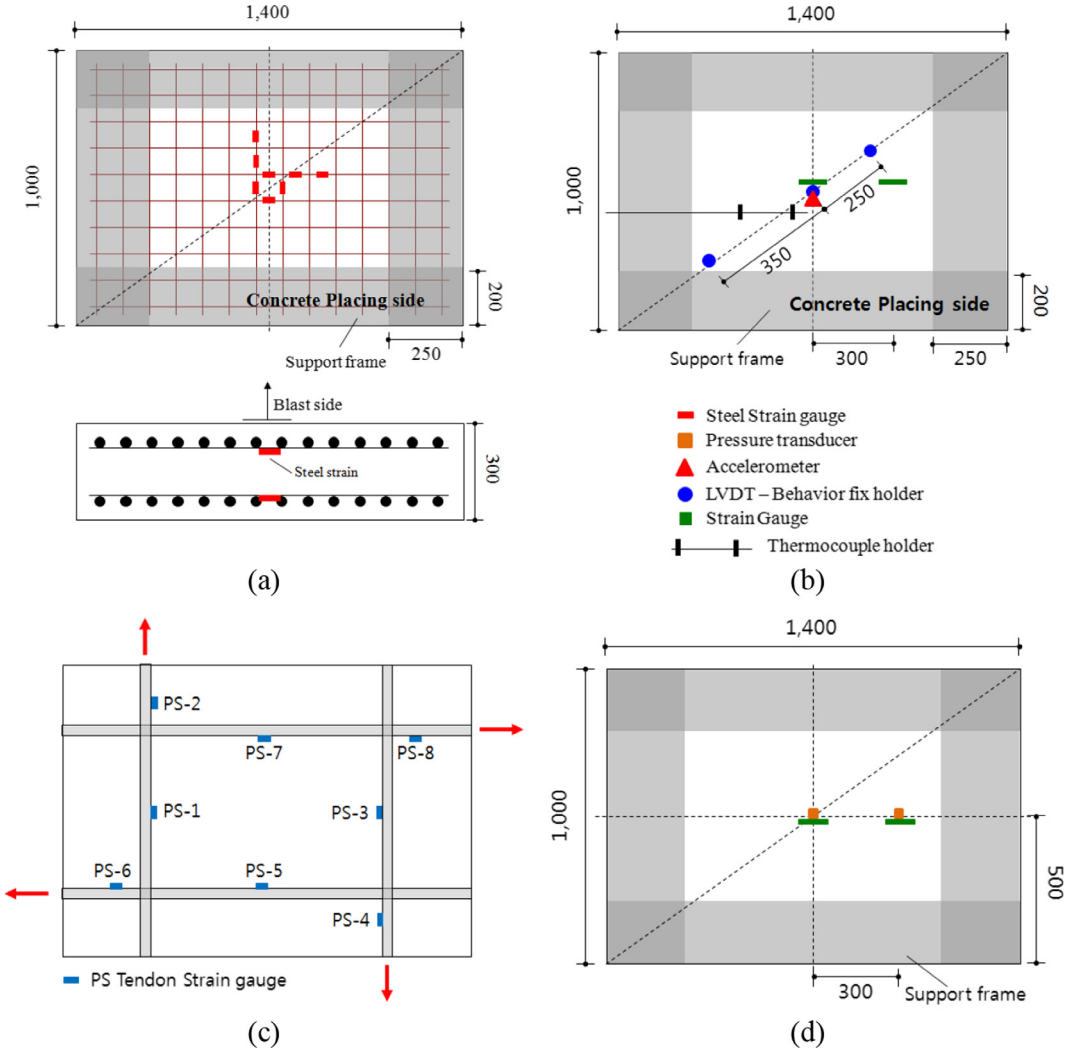


**Fig. 7.** Sensor locations of the specimen: (a) Steel strain gauge; (b) LVDT and accelerometer; (c) PS tendon gauge; (d) Pressure and concrete gauges.


**Fig. 8.** Overall blast test setup and measurement equipment photos: (a) Placed concrete specimen; (b) LVDT.

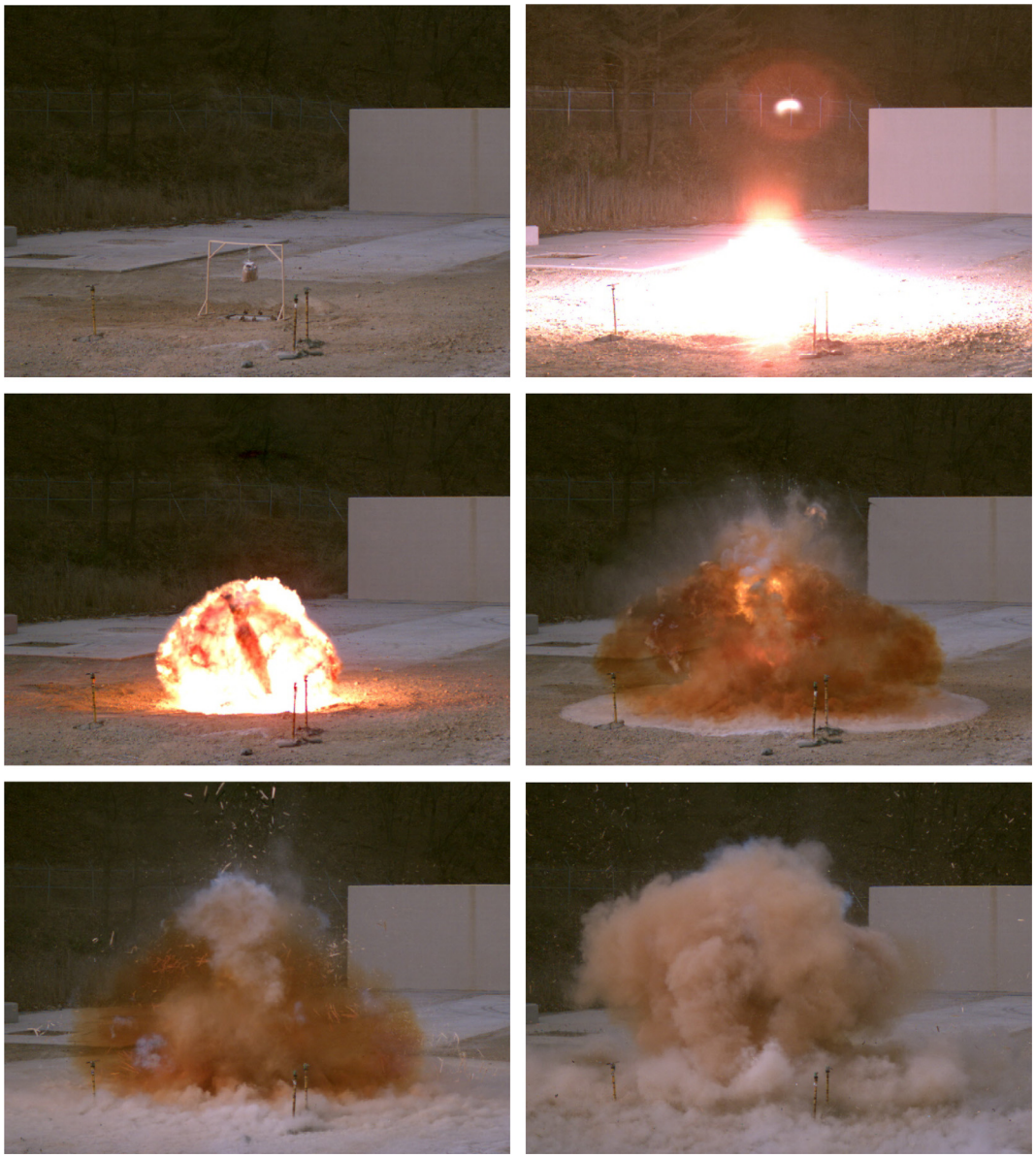

**Fig. 9.** Blast test photos from ANFO 25 kg explosion.

**Table 3**
ConWEP calculated overpressure and impulse from ANFO 25 kg with standoff distance of 1 m.

| Values | Incident | Reflected |
|---|---|---|
| Overpressure (MPa) | 0.3028 | 1.1466 |
| Impulse (MPa-msec) | 0.3021 | 0.8170 |
| Arrival time (msec) | 3.701 | |
| Positive phase duration (msec) | 4.611 | |
| Shock front velocity (m/s) | 641.299 | |
| Peak dynamic pressure (MPa) | 0.227 | |
| Peak particle velocity (m/s) | 384.962 | |

concrete specimen, an accelerometer was attached to the lower surface at the center of the specimen. For data acquisition, Dewe 1201 and Dewe 2600 from Dewetron, which can collect signals at a relatively high sampling rate of 200–500 kHz, equivalent to 10,000 times faster than static measurement equipment or general dynamic measurement equipment, were used. Generally, the sampling rate of high strain rate compatible LVDT is approximately 200,000–500,000 data acquisitions per second. Therefore, in this study, 500 kHz is used for the LVDT as well as pressuremeter and accelerometer. Also, the sampling rate of 200 kHz was used for rebar and concrete strain gauges. For high speed camera, a 5000 frames per sec capture setting was used. After the blast test, crack and damage patterns of the specimens were recorded. The tested specimen removal work was performed by entering the hollow space underneath the specimen created by the support structure.

### 3.3. Blast test procedure

Based on the aforementioned measurement system, the procedure of the blast test was conducted as follows. Prior to the test, steel plates that will connect the LVDTs and the specimen were installed. Then, the specimen was placed on the support structure to be aligned with the connecting part of the steel plate mounted in the specimen and LVDT in the center of the specimen. The wires to the measurement gauges were connected and calibrated to check whether signals are transmitting properly at the measurement locations. If no abnormal signals were found, the specimen was fixed to the support structure using C-clamps, impact absorbing rubber pad, and steel angle. The ANFO explosive was fixed 1 m away from the specimen using pre-manufactured square lumber hanger, as shown in Fig. 8(a), to induce a free air blast. Once the ANFO explosive was hanged on the hanger, a primer-inserted subsidiary charge was installed at the center of the explosive to induce a complete explosion. Since a blast pressure load can be significantly affected by environmental conditions such as wind velocity, temperature, and relative humidity, the test site climate conditions were carefully monitored and recorded. During the test, since the application of blast pressure is followed by high temperature fireball and roaring sound, the test was performed at a location where the blast pressure effect was minimal. After the explosion, the gauges placed at the lower surface of the specimen were removed, following the reverse order of the gauge installation. The final connection state of the gauges was checked to determine whether signals were reliable or not. Then, specimen was moved to a storage site and the failure patterns examined. The crack and damage patterns of the upper and lower surfaces of the specimens were marked using a specially manufactured acryl grid plate.

## 4. Blast test result discussions

### 4.1. Blast pressure load

The high speed camera photos of actual ANFO blast showing an explosive energy diffusion at a very high rate are shown in Fig. 9.

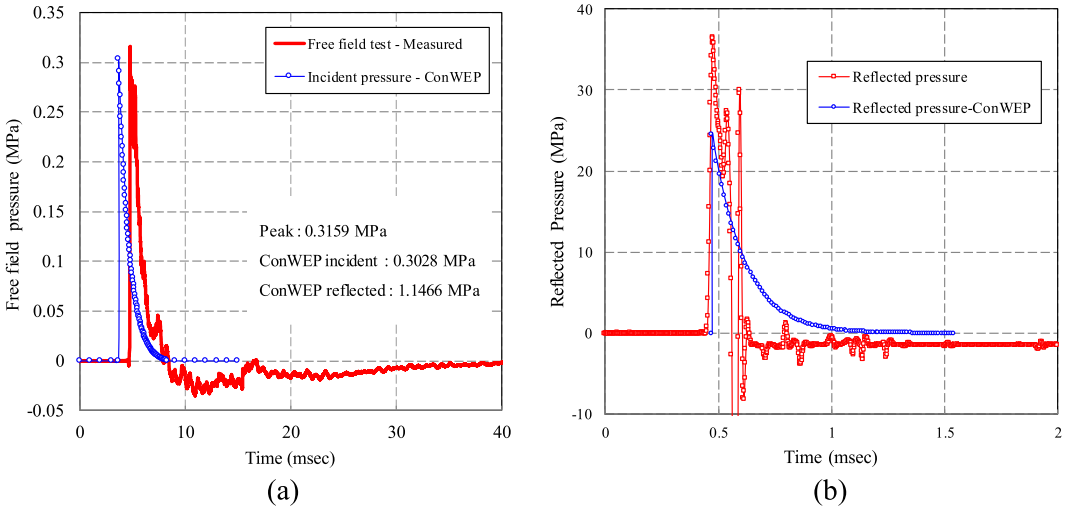


**Fig. 10.** Measured and calculated blast pressure of ANFO 25 kg: (a) Free field pressure; (b) Reflected pressure.

**Table 4**
Summary of overpressure and impulse from blasting of ANFO 25 kg with 1 m standoff distance.

| Specimens | Environment | | Free Field Pressure | | |
|---|---|---|---|---|---|
| | Temp. (°C) | Humid (%) | Peak Pressure (MPa) | Duration | Impulse (MPa·msec) |
| ConWEP | – | – | 0.3028 | 3.701 | 0.3021 |
| RC | 18.3 | 25 | 0.3159 | 3.232 | 0.3206 |
| PSC(B) | 9.6 | 38 | 0.4043 | 3.236 | 0.3448 |
| PSC(D) | 21.6 | 12 | 0.3838 | 3.272 | 0.3268 |
| PSRC(B) | 14.8 | 41 | 0.3671 | 4.192 | 0.3464 |
| PSRC(D) | 19.0 | 13 | 0.4176 | 4.342 | 0.3609 |

As shown in Fig. 9, the fire ball was relatively small for ANFO. However, severe toxic gas engulfed the test site after the explosion, indicating that ANFO diffuses energy mainly in the form of high temperature and high pressure gas.

The calculation results of blast pressure load estimated at the concrete specimen using ConWEP program from UFC3-340–1 are tabulated in Table 3. A comparison between the results measured from a pressuremeter installed for measuring a free field incident

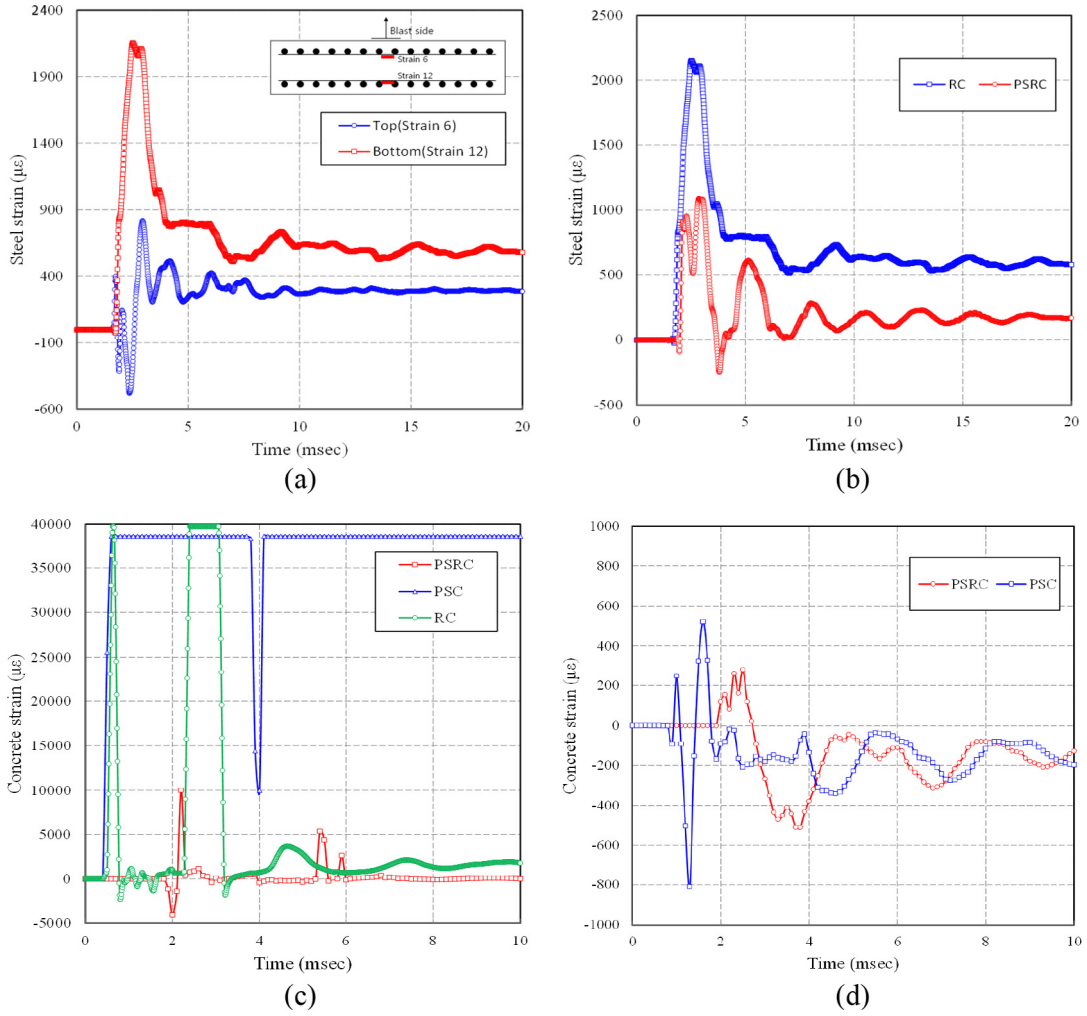


**Fig. 11.** Measured strain results of the specimens: (a) Steel strain of RC; (b) Steel strain of RC, PSRC (Bottom side); (c) Concrete strain (Top side); (d) Concrete strain (Bottom side).

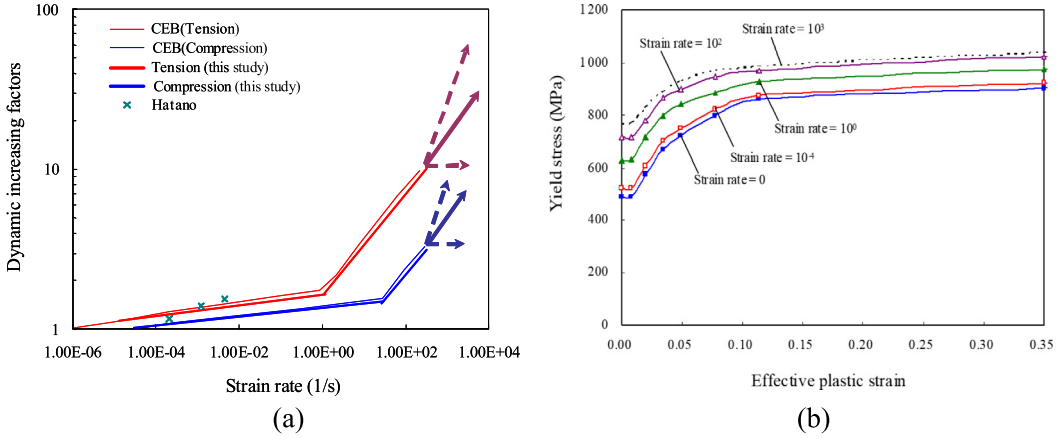


**Fig. 12.** Dynamic increasing factor and yield stress curves: (a) Strength enhancement due to high strain rates on concrete; (b) Relation of effective plastic strain-steel yield stress.

pressure at 5 m away from the specimen and calculated using ConWEP is shown in Fig. 10(a). Peak pressure and impact magnitude calculated by ConWEP were 0.3028 MPa and 0.3021 MPa-msec, respectively, while those measured from a free field pressuremeter were 0.3159 MPa and 0.3206 MPa·msec, respectively. The comparison indicates that the measured free air blast pressure was 4.33% larger in pressure load and 6.12% larger in impulse compared to the values calculated by ConWEP. Blast pressure load applied to the concrete specimen measured from pressure gauge attached to the specimen is compared with that calculated using ConWEP. During the test, most of pressure gauges were damaged by the blast pressure, which caused difficulties in data acquisition. However, as shown in Fig. 10(b), the pressure gauge results showed a relatively similar trend as the far field pressure data. It is important to note that the experimental blast pressure result was approximately 11.3 MPa higher than the ConWEP calculated. The difference in the results was due to various test site factors such as wind speed and direction, humidity, etc at the time of the test as shown in Table 4. Also, ANFO explosive mold shape caused deviations in the blast pressure magnitude. From the past experimental study published results, this type of error is commonly expected from blast tests [17,18].

**Table 5**
Concrete strength enhancement factor.

| Specimens | Strain rate (1/msec) | DIF ($\gamma_f$) |
|---|---|---|
| RC | 4.4531 | 1.3979 |
| PSC(B) | −4.4515 | 2.5775 |
| PSC(D) | −5.9102 | 2.8182 |
| PSRC(B) | 1.6792 | 1.3596 |
| PSRC(D) | 0.0026 | 1.2508 |

### 4.2. Strains

Blast behaviors of the specimen can be investigated further through evaluating the strain data obtained from the lower rebar. Fig. 11(a) shows a graph of strains measured from the gauges installed at the tension part in the upper and lower rebars of RC specimen. As verified in the result, both upper and lower rebars had mostly tensile strains from blast loading.

Concrete strains were measured from two strain gauges attached to the upper and lower surfaces of RC and PSC specimens as shown in Fig. 11(c) and (d). The strain data obtained from these gauges showed strain of more than 35,000 με from the blast pressure, and the same strain was maintained for a certain time duration. Based on these results, it can be judged that the strain exceeded the strain gauge capacity.

As shown in Fig. 11(b), the comparison of the strains measured at the centers of the RC and PSRC specimens showed that both exceeded the yield point. RC and PSRC specimens had the

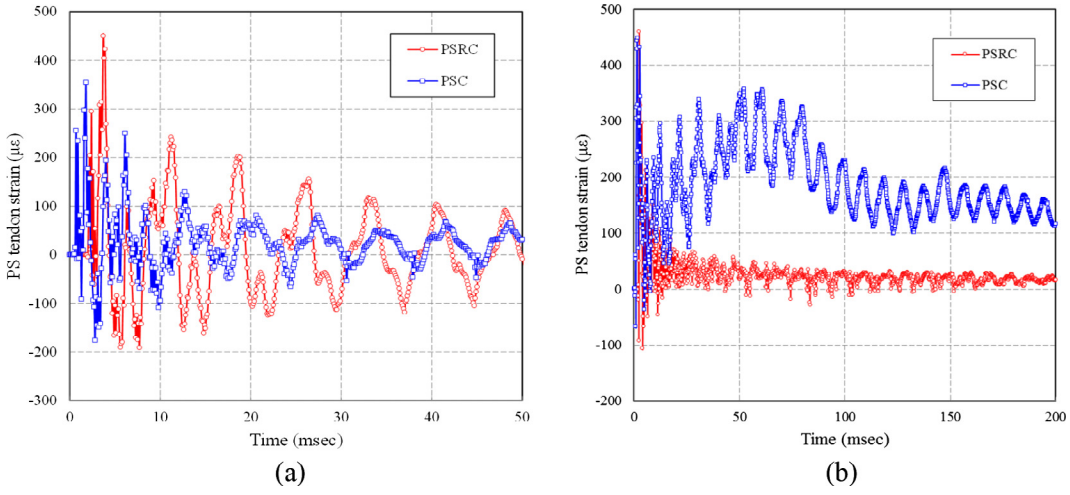


**Fig. 13.** Measured prestressed tendon strain results: (a) PS tendon strain-Lateral (PS-1); (b) PS tendon strain-Longitudinal (PS-7).

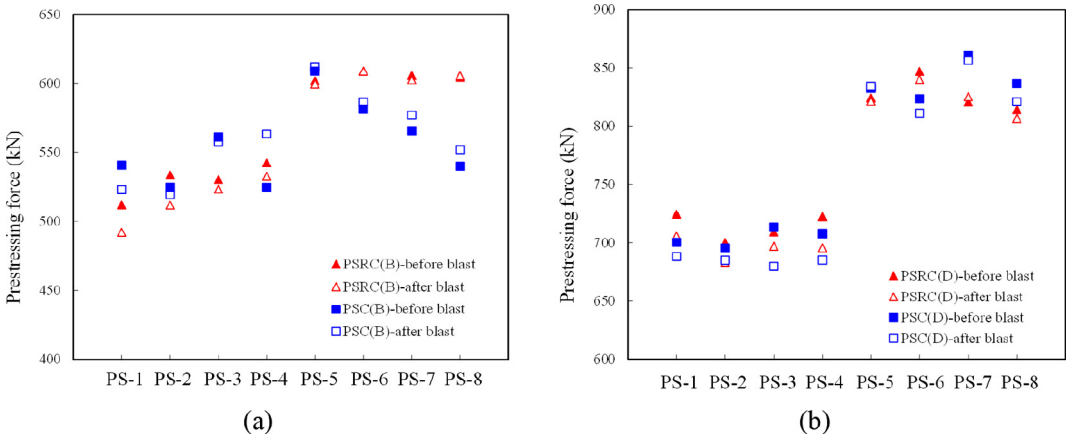


**Fig. 14.** Measured prestressing differences force in PSC and PSRC specimens; (a) PS tendon differences-(B); (b) PS tendon differences-(D).

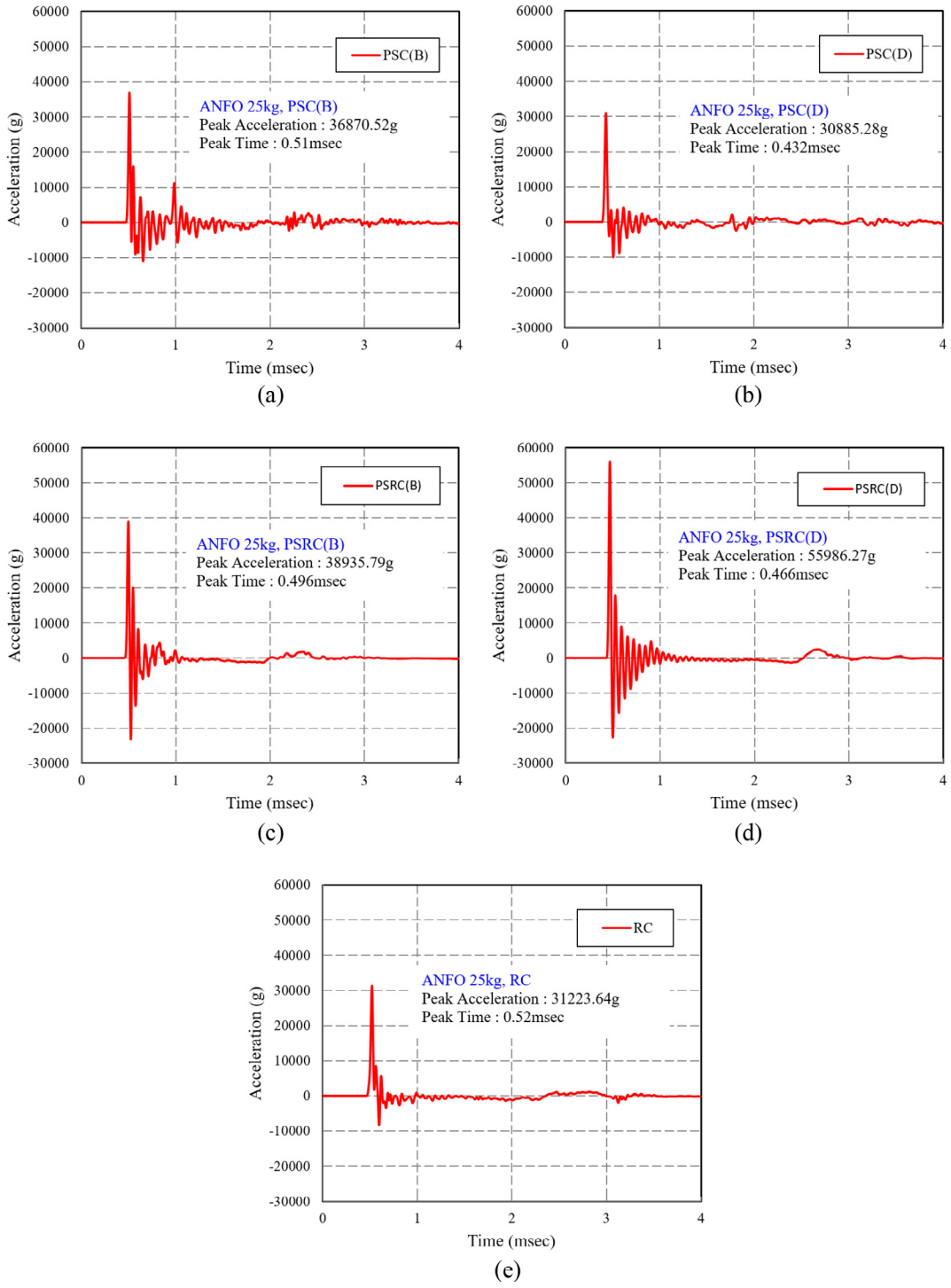


**Fig. 15.** Measured Peak acceleration result of the specimens: (a) PSC(B); (b) PSC(D); (c) PSRC(B); (d) PSRC(D); (e) RC.

**Table 6**
Summary of maximum and residual deflection experimental results. [Unit: mm]

| Values | Center | | 250 mm | | 350 mm | | Interface area |
|---|---|---|---|---|---|---|---|
| | Max. | Resi. | Max. | Resi. | Max. | Resi. | |
| RC | 13.80 | 3.32 | 10.58 | 2.90 | 9.91 | 2.33 | 1.0 |
| PSC(B) | 7.14 | 1.39 | 6.73 | 0.34 | 6.53 | 0.15 | 0.646 |
| PSC(D) | 6.48 | 2.10 | 5.98 | 1.10 | 3.87 | 0.91 | 0.646 |
| PSRC(B) | 8.79 | 1.13 | 7.40 | 1.04 | 6.61 | 0.86 | 1.646 |
| PSRC(D) | 7.96 | 0.95 | 6.69 | 0.54 | 6.00 | 0.27 | 1.646 |

maximum steel strain of 2154 με and 815 με, respectively, indicating that the PSRC reinforced with PS tendon had much smaller strain than that of the RC specimen. The strain results showed that the rebar and concrete strains closely reflect the damage degree of the specimens. If the strain values are converted to a stress values using Hook's Law, the strength increase due to dynamic impact factor (DIF) can be calculated and can be used for the calibration of DIF coefficient. Since DIF coefficient comes from the effect of inertia DIF coefficient is dependent on strain rate, acceleration, dynamic deflection, etc of the specimens under blast loading. However, in this study, DIF coefficient used in the simulation was obtained solely using the strain rate data of the tested specimens.

Since concrete behavior under blast load cannot be accurately predicted by models using static stress-strain relations, dynamic high strain rate effect related constitutive models have to be used. Also, the concrete strength increase with the increase in strain rate can be obtained by multiplying the strength enhancement factor. Kim et al. (2007) proposed the strength enhancement coefficient according to the strain rate based on CEB-FIP and experimental results as shown in Fig. 12(a). In a blast explosion, the strength enhancement factor was extended to exhibit strain rates up to 3E +02 $s^{-1}$. As shown in Fig. 12(b), the stress-strain relations of rebar with respect to the strain rate is shown by using a multilevel plastic model, which can consider the strain rate effect [28]. As shown in Table 5, the strain rate was derived from the deflection, strain, acceleration data, etc. In addition, the dynamic increasing factor (DIF) according to the maximum strain rate was obtained by using the strength increase coefficient value given in the previous studies [28,29]. This strength increasing factor is extended based on the experimental results so that the applied coefficients can be used up to high strain rates. DIF according to the maximum strain rate of each specimen are summarized in Table 5 where the derived DIF values are applied to the simulation.

### 4.3. Prestressing force loss

Strains measured from PS tendons were different from those of rebars. As shown in Fig. 13(a) and (b), a strain up to 300 με was

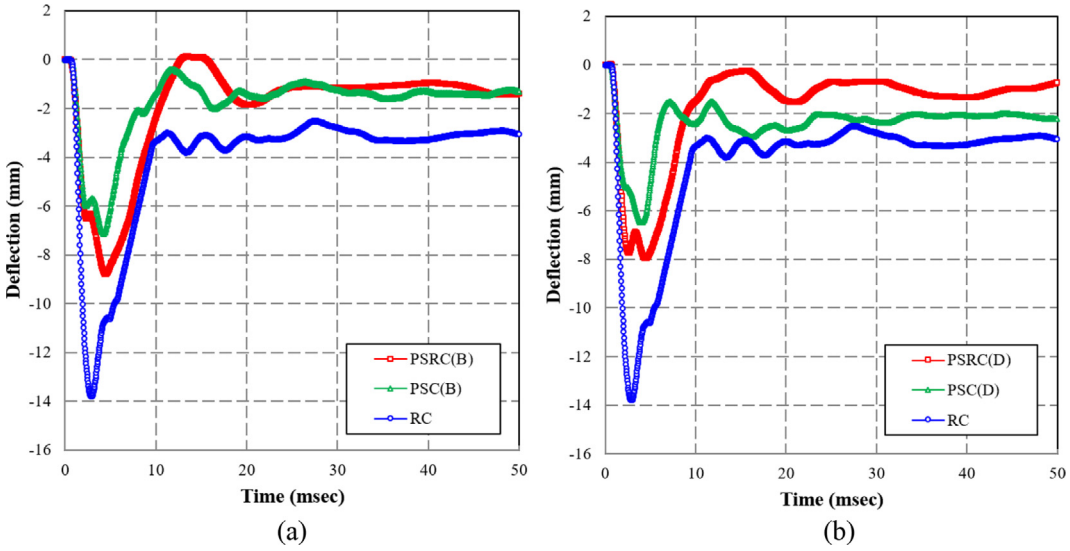


**Fig. 16.** Measured time-deflection curves: (a) Type B; (b) Type D.

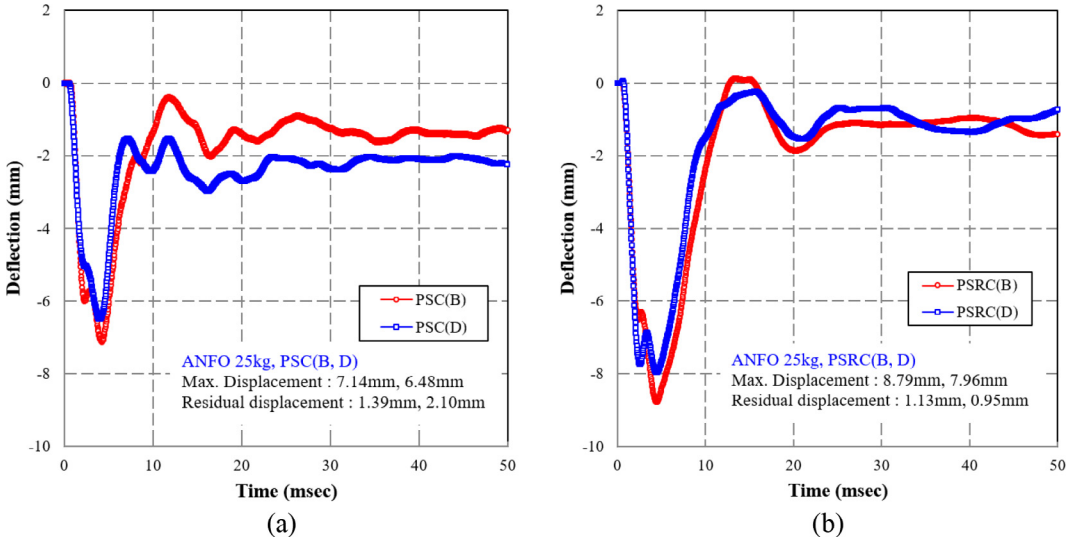


**Fig. 17.** Measured maximum deflection for PS force variation: (a) Maximum and residual deflection of PSC specimens; (b) Maximum and residual deflection of PSRC specimens.

observed in the PS tendon during blast loading with continuous trembling strain phenomenon, even after rebar and concrete strains stabilized. The effect of variations in prestressing force of PSC and PSRC specimens from blast loading were evaluated from PS tendon strains in shorter (PS-1-4) and longer (PS-5-8) dimensional directions, which are shown in Fig. 14(a) and (b). Both PSC and PSRC specimens showed prestressing force loss in both the shorter and longer dimensional directions. At the instant of blast load application, prestressing force increased instantaneously due to the great impulse load, but a prestressing forces in both the shorter and longer directions reduced to 17 kN–26 kN and 2 kN–12 kN, respectively, due to the PS force release phenomenon as the specimen deflection stabilized.

### 4.4. Accelerations

The acceleration behavior of the specimens subjected to the blast pressure was measured by an accelerometer. As shown in Fig. 15, when blast explosive of ANFO 25 kg was detonated, 31223.64 g, (30885.28–36870.52)g, and (38935.79–55986.27)g of accelerations were generated in RC, PSC, and PSRC specimen, respectively. The results showed that relatively higher acceleration occurred in the specimens with PS tendons due to greater structural stiffness from prestressing. Also, PSRC specimens showed higher acceleration than PSC specimens due to the higher structural stiffness contribution from 2 layers of grid rebars. However, all of the acceleration results are within the margin of error

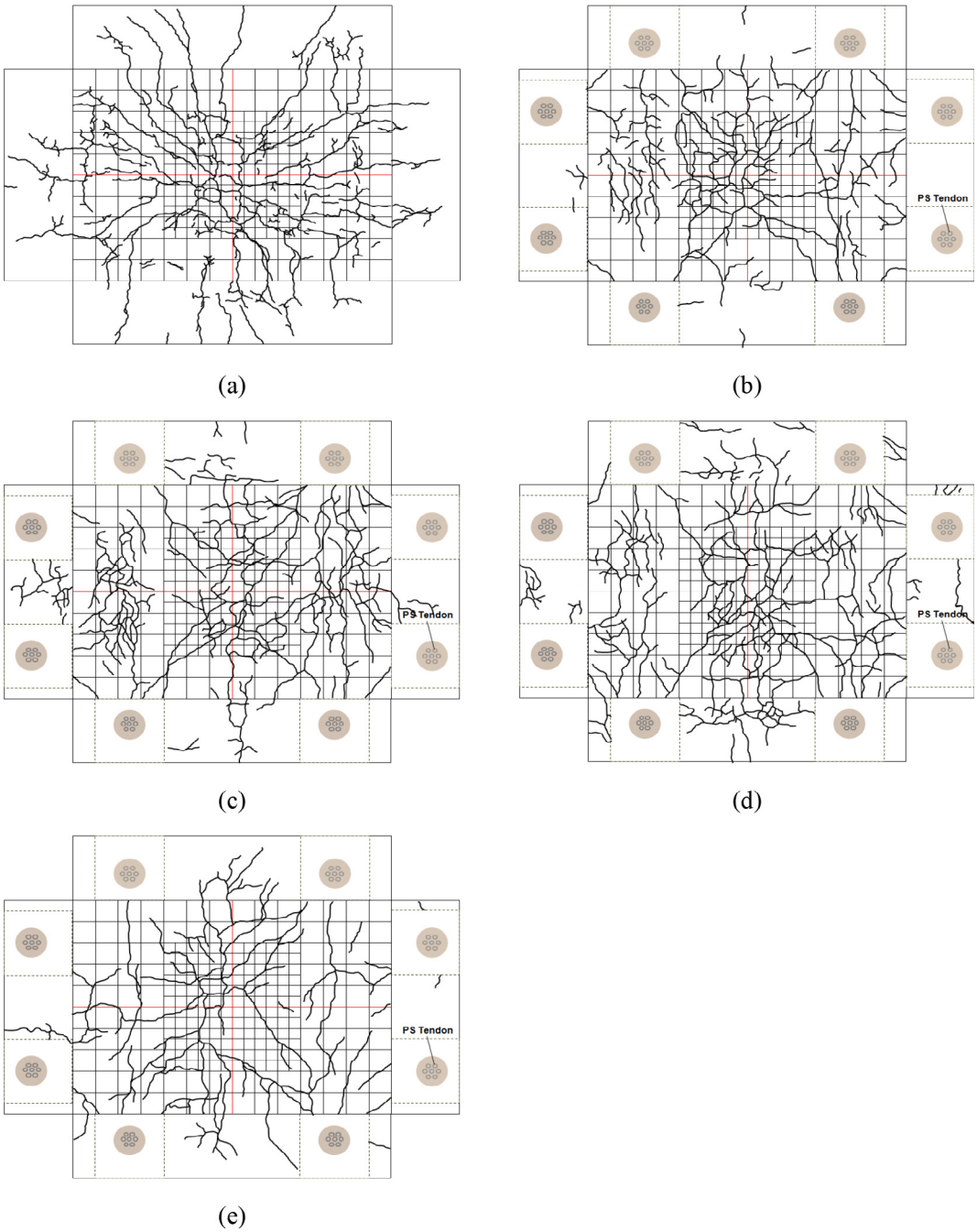


**Fig. 18.** Damaged of the bottom surface specimens from blast loading: (a) RC; (b) PSC(B); (c) PSC(D); (d) PSRC(B); (e) PSRC(D).

allowed in this type impulse loading condition. Most of the original structural stiffness is maintained without significant damage, even for highly accelerated specimens. It can be inferred that the specimen is behaving elastically. Therefore, the acceleration results indirectly show that the PSRC specimen has much higher blast resistant capacity than RC and PSC specimens.

### 4.5. Load-deflection relations

The maximum deflection and deflection behavior were measured using an LVDT installed at the center of bottom surface in the concrete specimen. Table 6 presents the maximum deflection and residual deflection of all specimens. Fig. 16 shows a graph of the maximum deflection for all specimen types. For RC specimens, the maximum and residual deflections were 13.80 mm and 3.32 mm, respectively, exhibiting the largest deflection among the three specimen types. As stated before, PSC(B), PSRC(B) and PSC(D), PSRC (D) represent the specimen with normal and high strength tendons applied with prestressing force of 510 kN and 820 kN, respectively. For PSRC(B) and PSC(B) specimens, the maximum deflections were 8.79 mm and 7.14 mm, respectively, and residual deflections were 1.13 mm and 1.39 mm, respectively. When maximum and residual deflections of PSRC(B) and PSC(B) are compared to RC deflection, they are 64% and 52%, and 34% and 42% less than those of RC specimens, respectively, as shown in Fig. 16(a). For PSRC(D) and PSC(D) specimens, the maximum deflections were 7.96 mm and 6.48 mm, respectively, and residual deflections were 0.95 mm and 2.10 mm, respectively, which are 58% and 47%, and 29% and 63% less than those of RC specimens, respectively, as shown in Fig. 16(b). For the consideration of PS force variation in the specimens PSC(B) and PSRC(B) specimens had no significant difference in the maximum and residual deflections and showed a difference within 1 mm, as shown in Fig. 17. It is important to note that the maximum deflection of PSC(B) specimens without rebars was 7.14 mm, which is 1.65 mm less than that of PSRC(B) specimen with rebars.

To further analyze these results, the deflections of the PSC(B) and PSRC(B) specimens were evaluated on the bottom surface at 250 mm and 350 mm from the center of the diagonal line from the center to the corner. For PSC(B) and PSRC(B) specimens, the maximum deflections at 250 mm and 350 mm point from the center were 6.73 mm and 7.40 mm, and 6.53 mm and 6.51 mm, respectively. The deflection results of PSC(D) and PSRC(D) specimens showed a similar trend as the results of PSC(B) and PSRC (B) specimens. It can be assumed that the maximum deflection difference was due to stiffness difference from interfaces created by embedded rebars and sheath tubes inside the specimen. Here, the interface ratio is the ratio of the interface volume to the total volume of the specimen. For the RC specimen, the surface interface volume of rebar and PSRC specimen is the surface interface volume of rebar and tendon. For the PSC specimen, the surface interface volume of the tendon is derived using the cross-sectional area formula, and the ratio of the total cross-sectional area is obtained. The interface volume value is in order of PSRC, RC, PSC, going from large to small. As presented in Table 6, when an interface between rebar and concrete in the RC specimen is normalized to 1.0, interfaces of the PSC and PSRC specimens are calculated to be 0.646 and

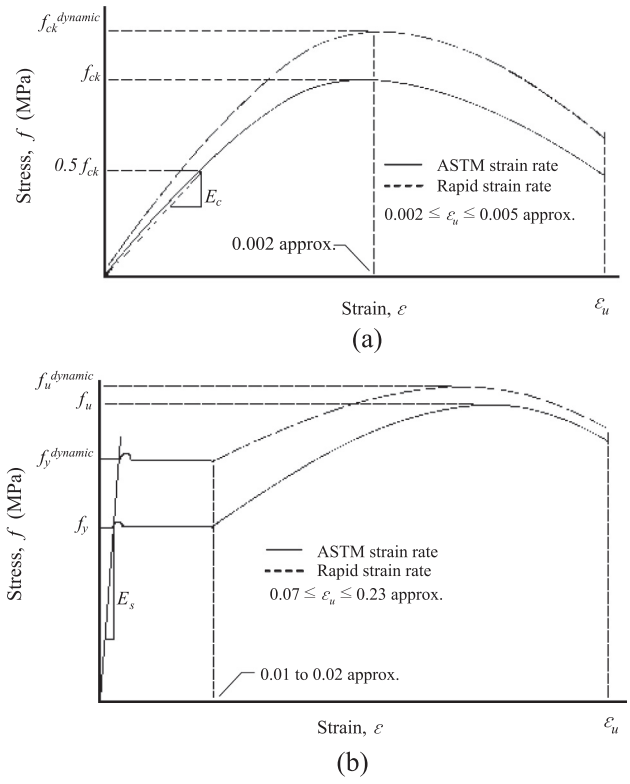


**Fig. 20.** Typical stress–strain curves for concrete and reinforcing steel (TM5-1300, 1990): (a) Stress-strain curve for concrete; (b) Stress-strain curve for reinforcing steel.

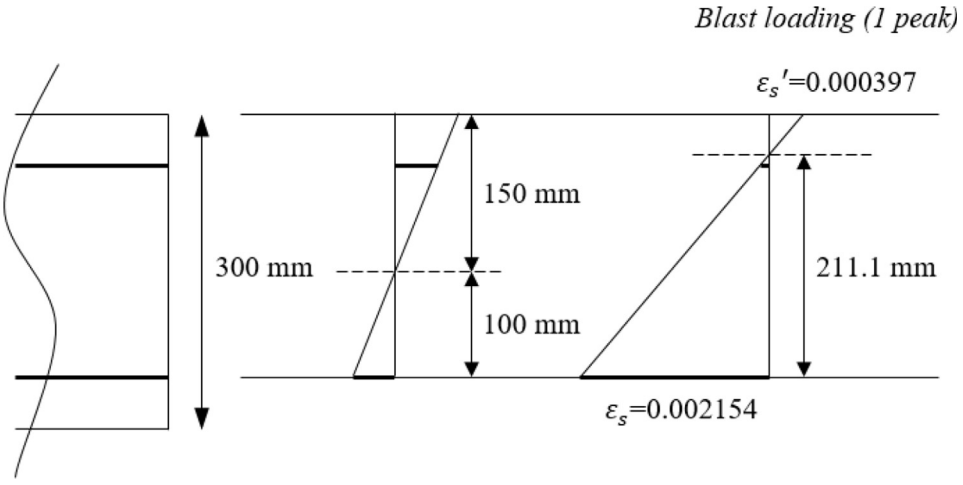


**Fig. 19.** The strain profile of the specimen under blast loading.

1.646, indicating that interface of the PSRC specimen is significantly larger than that of the PSC specimen. This difference in rebar interface ratio increased ductility of the specimen under blast loading, thereby improving blast resilience and resistant capacity. Therefore, in this study, unbonded prestressed concrete specimens (PSC, PSRC) without grouting behave in brittle manner compared to RC specimens. But, the increase in interfaces and voids inside the concrete due to the rebars, led to reduction in the concrete volume that can withstand large instantaneous blast pressure large deflection. The above study results imply that blast resistant capacity of the specimen are effected by various parameters, and other test results in addition to deflection and penetrated depth must be considered in evaluating the blast resistant capacity, such as crack shape, energy absorption, damage area, and residual structural performance.

### 4.6. Crack patterns

After the blast test, crack pattern of the specimen was marked as shown in Fig. 18. The upper surfaces of all specimens where blast pressure was directly applied showed no considerable damage and little cracks. The behavior of the specimen is analyzed according to the measured strain data. As shown in Fig. 19, when the blast load was applied, lower and upper rebar strain (1 peak) was 0.002154 and 0.000397, respectively, indicating that lower rebar exceeded yield strain of 0.002. The strain profile shows that the specimen was dominated by the tension behavior. Due to a minute compressive strain on the top compressive region of the specimen, no crack damage occurred, while significant macrocracks were observed on the bottom tensile region. Due to the characteristics of ANFO explosion pressure, only pure pressure load was applied to the specimen. As shown in Fig. 18(a), the lower surface of the RC specimen had radial cracks along the shape of the yield line of the concrete plate and macro shear cracks at the side. No significant spalling was found at the lower surface. The crack patterns indicated more damage has occurred in RC specimen compared to PSC and PSRC specimens. In addition, PSC and PSRC specimens showed more shear resistance due to their higher structural rigidity, because no shear cracks were found at the side surface of PSC and PSRC specimens. In particular, the specimens with PS tendons showed a crack along the shorter dimensional direction in the specimen where compressive force was generated, unlike in the RC specimens.

## 5. Numerical simulation verification

For the in-depth verification of the blast protective performance of PSC panel, finite element (FE) simulation was conducted to calibrate blasted loaded prestressed panel using the blast test results. The FE simulation tried to ensure higher accuracy than standard FEA methods by using LS-DYNA explicit FEA with a high-fidelity physics-based (HFPB) approach. In the HFPB FE simulation for concrete structures under extreme loading, a concrete damage model was applied considering strain rate and strength modification due to blast loading effect and multi-faceted reinforced bar plasticity model. The simulation models of RC, PSC, and PSRC specimens were modeled equivalently with the blast tested concrete panels.

Since the tests were performed outdoor, variations in temperature, wind velocity, relative humidity, etc can be viewed as the changes in test site conditions. Therefore, the data obtained from the tests can be viewed as the data effected by environmental

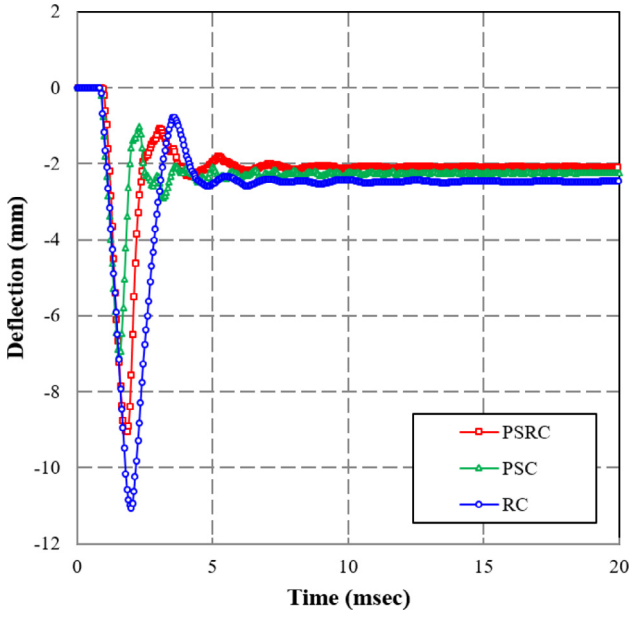


**Fig. 22.** Analytical results of blast loading.

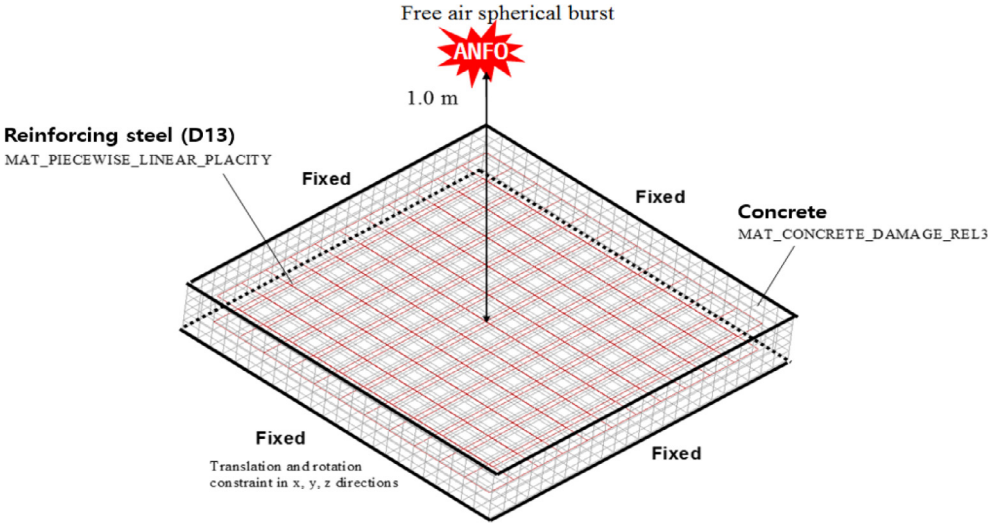


**Fig. 21.** FE simulation model for LS-DYNA.

conditions. Since the simulations model was calibrated using the data, the simulation model can be viewed as environmental condition varying model in average sense. Other than this type of indirect implementation in HFPB simulation, the simulations performed after the calibration cannot include the environmental condition variations.

### 5.1. Finite element model and boundary condition

To perform blast FE simulation on concrete panel models, it is necessary to apply real blast load rather than quasi-static load. Concrete and steel materials response under blast loading is quite different from that of materials in a static state. As loading rate increases, material strength tends to increase. This strength increasing effect has been confirmed through the previous researches about the relationship between the strain rate variation and the increase in material strength [30–34]. The strength increasing effect of concrete and steel from the increase in strain rate are shown in Fig. 20 [23]. The modified stress-strain relation is used for the blast simulation.

The calibration of the simulation tool was performed by using LS-DYNA explicit analysis program by verifying the data obtained from the blast test. The panel analysis model applied in this study is shown in Fig. 21. The blast load was modeled in a form of pressure applied on a top surface of the panel model. The displacement in the x, y, and z directions and the rotation of all four sides of the panel model were restrained. The concrete and the rebar model were implemented as solid element (∗ELEMENT_SOLID) and beam element (∗ELEMENT_BEAM), respectively. Also, LS-DYNA explicit code offers concrete material model cards. Concrete constitutive models in LS-DYNA are defined by multiple and complex parameters. However, these models are poorly documented in its theoretical and keyword manuals [35]. Material Model 16 (MAT_PSEUDO_TENSOR) is a pseudo-tensor geological model with an option for reinforcement. The model offers two major characteristics. One is a simple pressure-dependent Mohr-Coulomb yield surface with Tresca limit. The other is "yield versus pressure" functions with the capability to transit from one curve to another. The latter is used with the damage scale option as suggested by the User Manual [35]. The state (EOS) type 8 equation is used, which describes the volumetric response of the material. Material Model 72 (MAT_CONCRETE_DAMAGE) is similar to Material Model 16 with additional parameters that include damage features. In this study, the concrete material model was implemented by using a material card MAT_CONCRETE_DAMAGE_REL3 (MAT_72R3). As an isotropic material model, the rebar material models were implemented by using a material card ∗MAT_PIECEWISE_LINEAR_PLASTICITY (MAT_24), which has strain rate effect and kinematic hardening characteristic. To apply prestressing force to tendons, the temperature induced shrinkage is used, because there is no direct way to apply presstressing force in concrete members in the LS-DYNA program. In order to apply prestressing force, prestressing tendons are constrained to concrete elements by CONSTRAINED_LAGRANGE_IN_SOLID option. The temperature induced strain, $\varepsilon_T$ was implemented to tendon beam elements using Eq. (2)

$$\varepsilon_T = \Delta T \alpha \tag{2}$$

where, $\alpha$ is the thermal expansion coefficient of tendon ($\alpha = 1 \times 10^{-5}/°C$) and is a temperature variation from the initial temperature. The temperature change is obtained by applying the strain compatibility condition between concrete and tendon using Eq. (3).

$$\Delta T \alpha - \frac{f}{E_s A_s} = \frac{f}{E_c A_c} \tag{3}$$

where, $E_s$ and $A_s$ are elastic modulus and cross section area of tendons, respectively, while $E_c$ and $A_c$ represent the corresponding values for concrete.

Given the prestressing force, $f$, $\Delta T$ can be obtained by Eq. (4).

$$\Delta T = \frac{f}{E_s A_s \alpha}\left(1 + \frac{E_s A_s}{E_c A_c}\right) \tag{4}$$

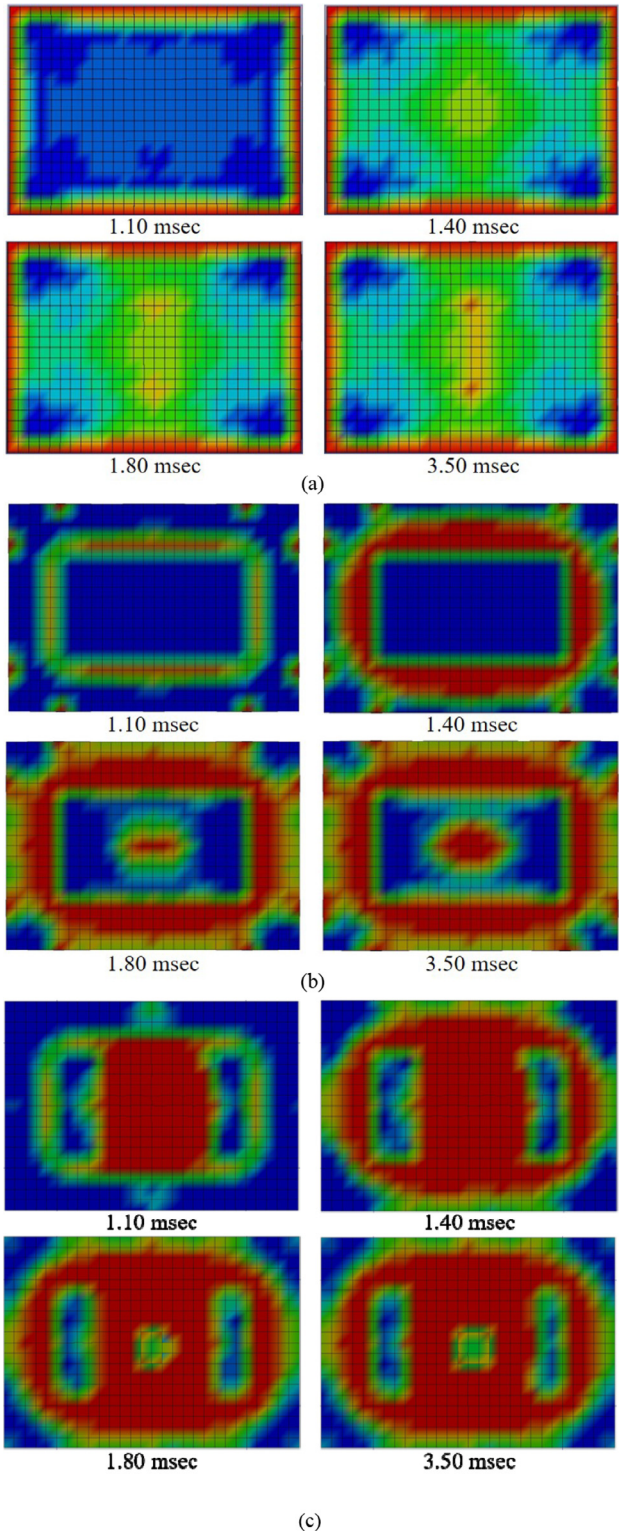


**Fig. 23.** FE analysis results for distribution of plastic strain: (a) RC; (b) PSC; (c) PSRC.

MAT_ADD_THERMAL_EXPANSION model is used for defining the temperature dependent material property for tendons. Along with this material option, the LOAD_THERMAL_LOAD CURVE option is used for defining temperature versus time curve. It is suggested that the prestressing force be applied using DYNAMIC_RELAXATION command option to initialize the stresses and deformation in the model. The prestressing force was applied to both initialization and transient analysis [36].

The boundary between PSC specimen and blast wave was implemented using LS-DYNA's Contact Algorithm (Contact Automatic One Way Surface to Surface command) based on material model incorporating constraint effect [22]. The blast loading model was applied by using a load card ∗LOAD_BLAST. Using the same load condition of that of the actual test, the maximum pressure was calculated from an ANFO 25 kg with a blast standoff distance of 1.0 m on the top surface of the specimen.

### 5.2. Blast simulation result discussions

Since the deflection behavior of concrete panel under blast loading is the most important result of the simulation, the maximum deflections from the blast pressure application on the specimens were measured and compared with those from the blast tests. Fig. 22 shows a graph of the maximum deflection for all specimen types. For the RC specimen, the maximum deflection was 13.29 mm, which is the largest maximum deflection among all of the specimens. For PSC and PSRC specimens, the maximum deflections were 7.06 mm and 8.93 mm, respectively, which are approximately 53.12% and 67.19% decrease compared to that of the RC specimen, respectively, due to increased member stiffness from prestressing. Fig. 23 shows the effective plastic strain on the bottom concrete surface of the specimens. Distribution of the plastic strain rate by specimen types verified that a considerable plastic

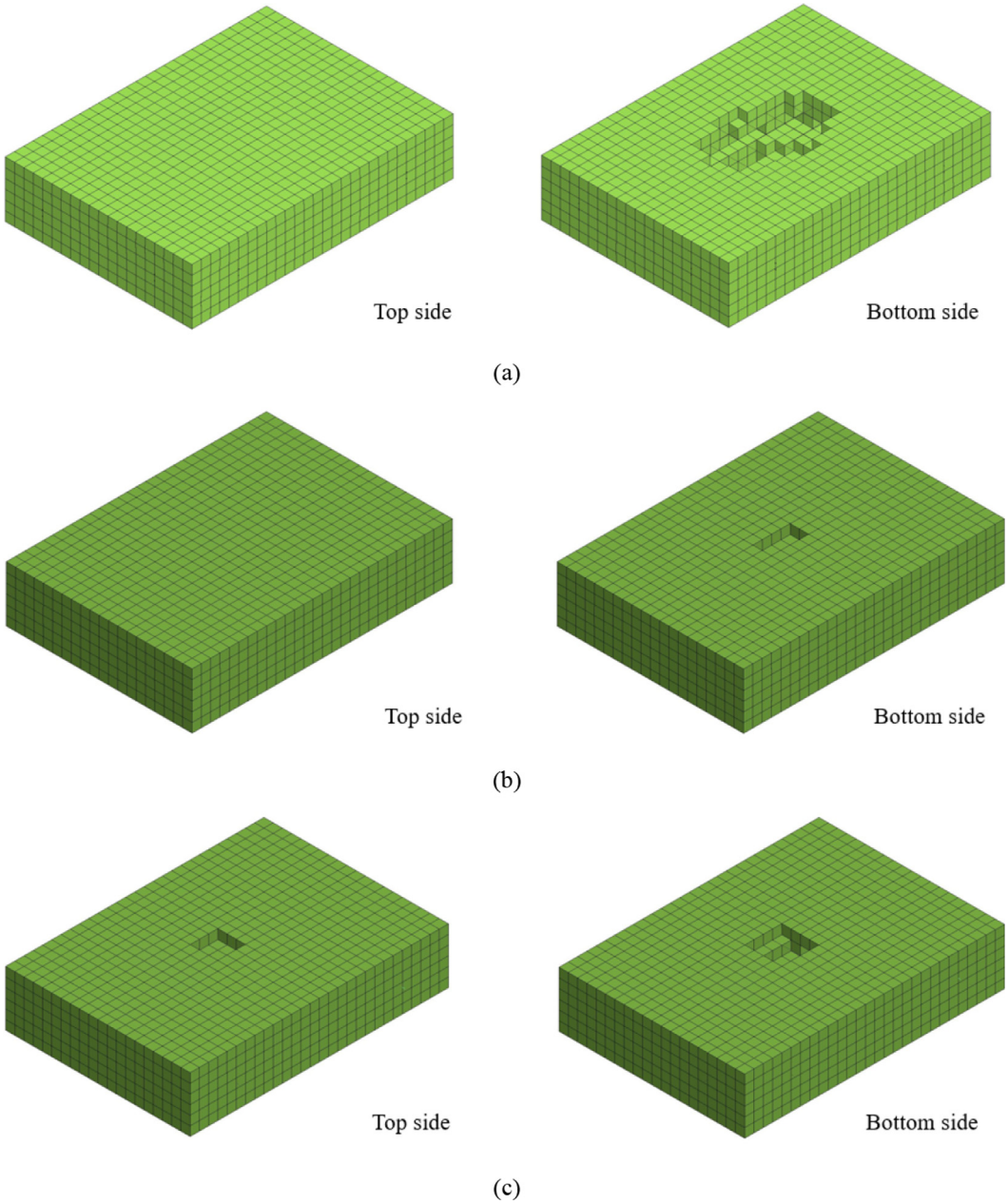


**Fig. 24.** FE analysis results for damage area: (a) RC specimen; (b) PSC specimen; (c) PSRC specimen.

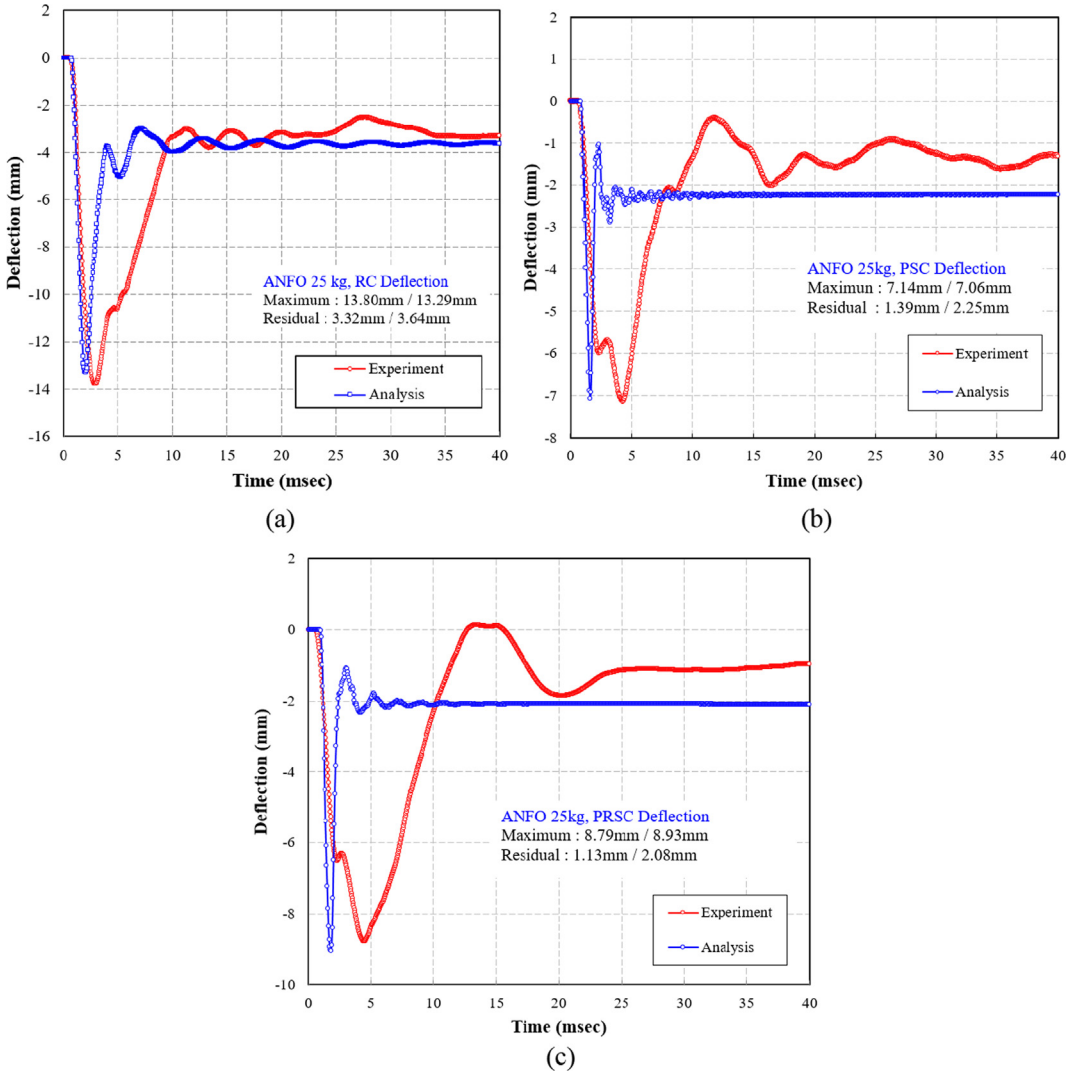


**Fig. 25.** Comparison of experimental and analytical results: (a) RC specimen; (b) PSC specimen; (c) PSRC specimen.

**Table 7**
Summary of experiment and HFPB analysis results.

| Value | Experiment | | HFPB analysis | | | |
|---|---|---|---|---|---|---|
| | Deflection (mm) | | Deflection (mm) | | Damage volume ($\times 10^6$ mm$^3$) | Damage rate (%) |
| | Maximum | Residual | Maximum | Residual | | |
| RC | 13.80 | 3.32 | 13.29 | 3.64 | 95.75 | 22.80 |
| PSC | 7.14 | 1.39 | 7.06 | 2.25 | 4.0 | 0.95 |
| PSRC | 8.79 | 1.13 | 8.93 | 2.08 | 4.75 | 1.13 |

**Table 8**
Typical failure criteria for structural elements of concrete structures.

| Element type | Material properties | Failure type | Criteria | Light damage | Moderate damage | Severe damage |
|---|---|---|---|---|---|---|
| Beam | Reinforced concrete ($\rho$>0.5%/face) | Global bending/Membrane response | Ratio of center-line deflection to span, $\delta/L$ | 4% | 8% | 15% |
| | | Shear | Average shear strain across section, $\gamma_v$ | 1% | 2% | 3% |
| Slab | | Bending/Membrane | $\delta/L$ | 4% | 8% | 15% |
| | | Shear | $\gamma_v$ | 1% | 2% | 3% |
| Column | | Compression | Shortening/height | 1% | 2% | 4% |
| Load-bearing wall | | Compression | Shortening/height | 1% | 2% | 4% |
| Shear wall | | Shear | Average shear strain across section | 1% | 2% | 3% |

strain occurred in the RC specimen, with the PSC and PSRC specimens having less plastic strain than the RC specimen. From the blast test simulation, the simulation results are analyzed to calculate damage volume and damage rate. The damage is defined as concrete strain exceeding allowable principle strain value of 0.01 in an element [36]. However, the erosion criteria of the concrete elements are different from each study. Therefore, in this study, the maximum principle strain at failure is incorporated in the finite element code, LS-DYNA. When the maximum principle strain exceeds the threshold value, the associated element is removed. The element erosion failure maximum principle strain of concrete model was set 0.04 based on experimental results, which is four times the threshold value for principle strain criteria in Jiang et al. (2015) [37].

Based on this definition, all of damaged concrete elements from the blast simulation are checked and accrued as a total damage volume. Also, after adding all of damaged element volume, a damage rate is calculated by dividing the damaged concrete element volume with the total concrete element volume. The damaged mesh configurations of RC, PSC, and PSRC specimens extracted from the blast simulations are shown in Fig. 24. The eliminated elements in the mesh are the elements that exceeded the maximum allowable strain limit using MAT_ADD_EROSION option in LS-DYNA program. In Fig. 24 RC model has significant well distributed damages from blast loading. However, PSC model shows less blast damage with damages located mostly in concrete near the prestressing tendons and along reaction supports. Especially, PSRC model has insignificant damage from the blast loading with a minor damage at the center of the specimen.

In the experiment, only damages from the blast can only be observed and measured from concrete surface of the specimen. However, in the simulation, damages can be quantitatively measured externally as well as internally, allowing the analysis to be much more precise and thorough in calculating overall blast damage rate of the specimens. When exactly same conditions used for the blast test are used for the blast simulation (i.e., ANFO 25 kg, standoff distance 1.0 m, concrete compressive strength 40 MPa, etc.), the damage volume and damage rate of RC, PSC, and PSRC are $95.75 \times 10^6$ mm$^3$ and 22.80%, $4.0 \times 10^6$ mm$^3$ and 0.95%, and $4.75 \times 10^6$ mm$^3$ and 1.13%, respectively. The damage rate of PSC and PSRC are 21.85% and 21.67% less than that of RC specimen, respectively. The simulation results showed that the prestressing force induced confinement effect in concrete significantly reduced the overall damage to the simulation specimens, showing that prestressing is an effective mean to increase blast resistance to concrete member. Also, the results showed that the current practice of using PSRC wall is better than RC wall against extreme loading scenarios in protecting the concrete containment vessels. The plastic strain rate distribution verified that the brittleness tendency of the specimen increased as stiffness increased due to prestressing, thereby showing more brittle behavior under blast loading.

### 5.3. Comparison between simulation and test results

The maximum and residual deflection results from the simulations are compared to the blast test results as shown in Fig. 25. For the RC specimen, the maximum and residual deflection from the simulation were 13.29 mm and 3.64 mm, respectively. As presented in Table 7, both maximum and residual deflection between the test and simulation showed an error within 4%.

For the PSC and PSRC specimens from the simulation, the maximum deflections were 7.06 mm and 8.93 mm, and the residual deflections were 2.25 mm and 2.08 mm, respectively. The PSC and PSRC specimens showed an error of within 2% for residual deflection between the tests and simulations. The residual deflection had slightly difference between the tests and simulations in the PSC and PSRC specimens due to the differences in instantaneous loss and recovery of prestressing forces in the tendons. As reported in previously published study results, the maximum deflection and recovery force can vary significantly under extreme instantaneous loading such as explosive shape, PS force magnitude at the moment of blast loading, etc [16–18]. However, these factors

**Table 9**
Blast assessment according to concrete compressive strength.

| Compressive strength | | Max. deflection (mm), $\delta$ | $\delta/L$ (%) | Damage criteria | Damage volume ($\times 10^6$ mm$^3$) | Damage rate (%) |
|---|---|---|---|---|---|---|
| RC | 30 MPa | 72.41 | 5.57 | Moderate damage | 196.125 | 46.67 |
| | 40 MPa | 13.30 | 1.02 | Light damage | 95.75 | 22.80 |
| | 50 MPa | 1.59 | 0.12 | Light damage | 70.875 | 16.875 |
| PSC | 30 MPa | 13.07 | 1.01 | Light damage | 13.875 | 3.30 |
| | 40 MPa | 7.06 | 0.54 | Light damage | 4.0 | 0.95 |
| | 50 MPa | 3.52 | 0.27 | Light damage | 1.0 | 0.24 |
| PSRC | 30 MPa | 17.54 | 1.35 | Light damage | 11.625 | 2.77 |
| | 40 MPa | 8.93 | 0.69 | Light damage | 4.75 | 1.13 |
| | 50 MPa | 8.37 | 0.64 | Light damage | 2.125 | 0.51 |

**Table 10**
Blast assessment according to standoff distance.

| Standoff distance | | Max. deflection(mm), $\delta$ | $\delta/L$ (%) | Damage criteria | Damage volume ($\times 10^6$ mm$^3$) | Damage rate (%) |
|---|---|---|---|---|---|---|
| RC | 0.5 m | 47.13 | 3.62 | Light damage | 420 | 100 |
| | 0.75 m | 24.74 | 1.91 | Light damage | 259.625 | 61.82 |
| | 1.0 m | 13.30 | 1.02 | Light damage | 95.75 | 22.80 |
| PSC | 0.5 m | 43.14 | 3.32 | Light damage | 60.625 | 14.43 |
| | 0.75 m | 18.57 | 1.43 | Light damage | 60.5 | 14.40 |
| | 1.0 m | 7.06 | 0.54 | Light damage | 4.0 | 0.95 |
| PSRC | 0.5 m | 41.25 | 3.17 | Light damage | 35.125 | 8.36 |
| | 0.75 m | 21.22 | 1.63 | Light damage | 15.125 | 3.60 |
| | 1.0 m | 9.04 | 0.70 | Light damage | 4.75 | 1.13 |

cannot be considered in the simulation using LS-DYNA since the prestressing force is constant throughout the simulation. Thus, these errors should be taken as inherent differences between the blast test and simulation. Therefore, other than these uncontrollable errors in simulations, it can be assumed that the blast simulation model is sufficiently calibrated to be used for the parametric study. For these reasons, magnification factor need to be used to compensate for the maximum displacement difference. A further study must be performed on this topic.

### 5.4. Damage assessment of concrete strength and blast standoff distance variations

The parametric study aims to perform the blast simulations of the panels for various standoff distance and concrete strength parameters. To verify the effect of blast behavior according to standoff distance, simulations of detonating 25 kg ANFO explosive at 0.5 m, 0.75 m, and 1.0 m standoff distance are performed. Also, simulations according to various concrete strength of 30, 40, and 50 MPa are performed to verify the blast behavior of the panels. The damage assessment considering a ratio of beam end rotation or deflection to the span length of the panel specimens is conducted according the method proposed by the ASCE (1999) as presented in Table 8.

The parametric simulation results are tabulated in Tables 9 and 10. The maximum and residual deflection according to changes in concrete compressive strength are shown in Fig. 26 and Table 9. For the RC specimen with a concrete strength of 30 MPa, the maximum deflection was 72.41 mm, exceeding the allowable maximum deflection of a panel or slab by ASCE (1999) of 40 mm. This deflection amounts to moderate damage that corresponded to $\delta/L = 4\%$, which can be considered as large damage. For the simulation results of RC specimens with concrete strength of 40 MPa and 50 MPa, the maximum deflections were 2.06 mm and 5.19 mm, respectively, which amount to minimal damage within $\delta/L = 4\%$. For the PSC and PSRC specimens, the maximum deflection tended to decrease as concrete strength increased. The PSC and PSRC specimens exhibited light damage within $\delta/L = 4\%$ at concrete strength of 30–50 MPa, which amounts to minimal damage. The trend of the results verified that prestressed concrete panel resistance against blast increased as the design strength of concrete increased. In contrast to the PSC and PSRC specimens, the blast resistance of RC specimen considerably decreased as concrete strength increased, which is shown in Fig. 26(a). The PSRC specimen showed smaller maximum and residual deflections as concrete strength increased.

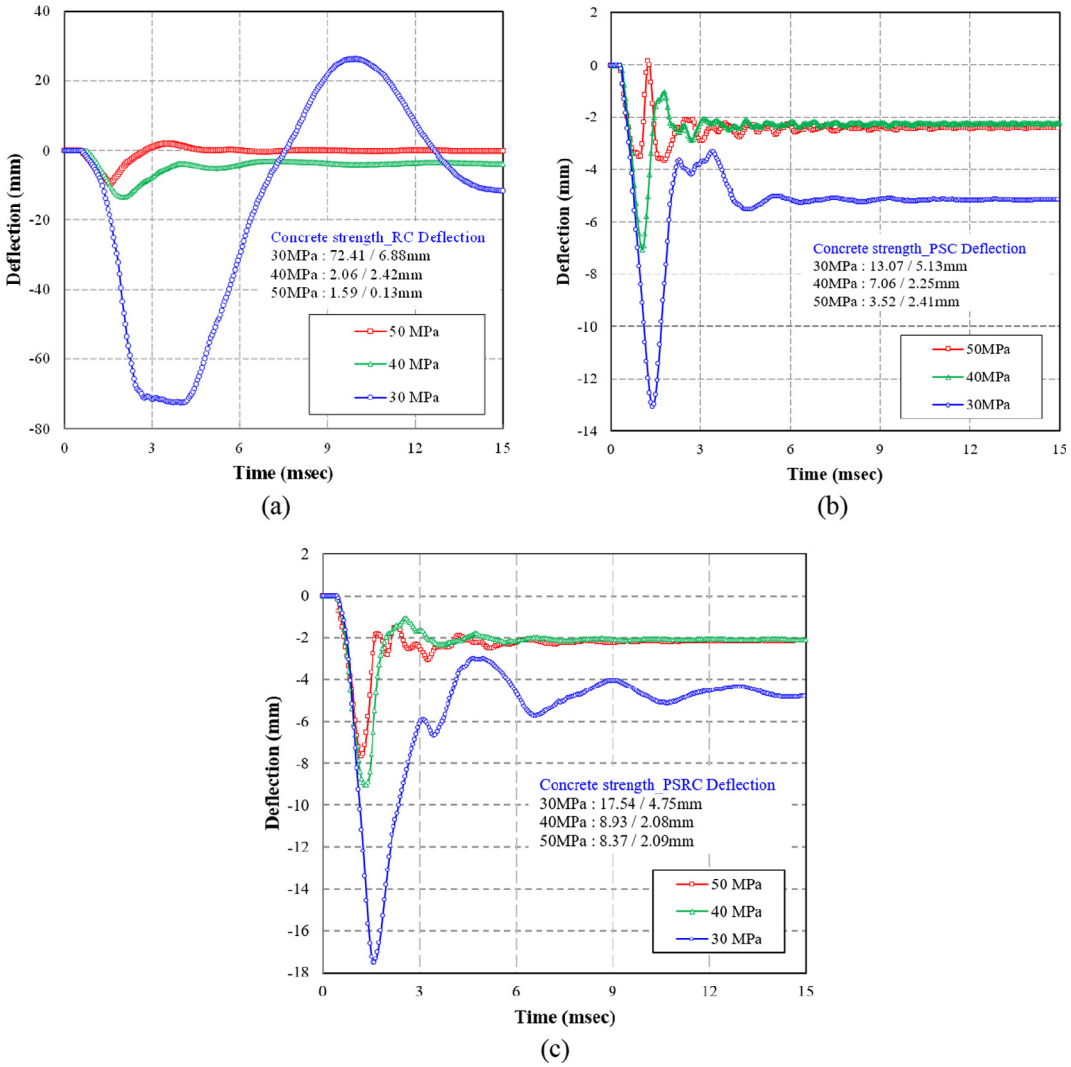


**Fig. 26.** Time-deflection curves according to concrete compressive strength: (a) RC specimen; (b) PSC specimen; (c) PSRC specimen.

For RC specimen, the damage volume and damage rate with concrete compressive strength of 30 MPa and 50 MPa are $196.125 \times 10^6$ mm$^3$ and 46.67%, and $70.875 \times 10^6$ mm$^3$ and 16.875%, respectively. On the other hand, for PSC and PSRC specimens, the damage volume and damage rate with concrete compressive strength of 30 MPa are $13.875 \times 10^6$ mm$^3$ and 3.30%, and $11.625 \times 10^6$ mm$^3$ and 2.77%, respectively. Also, the damage volume and damage rate with concrete compressive strength of 50 MPa showed $1.0 \times 10^6$ mm$^3$ and 0.24%, and $2.125 \times 10^6$ mm$^3$ and 0.51%, respectively. As the concrete compressive strength increased the blast resistance to explosive load improved. The similar tendency is shown in the damage assessment results presented in Table 9. The damage rate of PSC and PSRC specimens with concrete compressive strength of 30 MPa and 50 MPa are 43.37% and 16.635%, respectively, which is 43.9%, and 16.365% less than that of RC specimen, respectively.

Fig. 27 and Table 10 show the simulation results according to standoff distance variation. When all the specimens were set to 0.5 m standoff distance, prestressing force recovery was not found, since the failure mechanism of elastic failure was observed, which means that the blast at a distance of 0.5 m is similar to contact blast detonation with a complete loss of resistance property of the structure as it displaces. The blast results at standoff distances of 0.75 m and 1.0 m showed smaller maximum deflection due to restraint force. The RC, PSC, PSRC specimens showed a maximum deflection of 47.13 mm, 43.14 mm and 41.25 mm at 0.5 m standoff distance, which can be evaluated as light damage since it is within a range of $\delta/L = 4\%$.

For RC specimen, the damage volume and damage rate with standoff distance of 0.5 m and 0.75 m are $420 \times 10^6$ mm$^3$ and 100%, and $259.625 \times 10^6$ mm$^3$ and 61.82%, respectively. Particularly, when the standoff distance was 0.5 m, it was confirmed that all of the elements were damaged, which is equivalent to the damage rate of 100%. On the other hand, for PSC and PSRC specimens, the damage volume and damage rate with standoff distance of 0.5 m are $60.625 \times 10^6$ mm$^3$ and 14.43%, and $35.125 \times 10^6$ mm$^3$ and 8.36%, respectively. Also, the damage volume and damage rate with standoff distance of 0.75 m of PSC and PSRC specimens are $60.5 \times 10^6$ mm$^3$ and 14.40%, and $15.125 \times 10^6$ mm$^3$ and 3.60%, respectively. The simulation results showed that the damage from the explosion becomes more serious as the standoff distance becomes closer. The damage rate of PSC and PSRC specimens with standoff distance of 0.5 m and 0.75 m are 85.57% and 47.42% and 91.64%, and 58.22% less than those of RC specimen, respectively. Therefore, the PSRC specimen is better than RC and PSC specimens in the blast resistance against extreme loading, due to the loss of prestressing force from impulse effect on tendons and the presence of rebar.

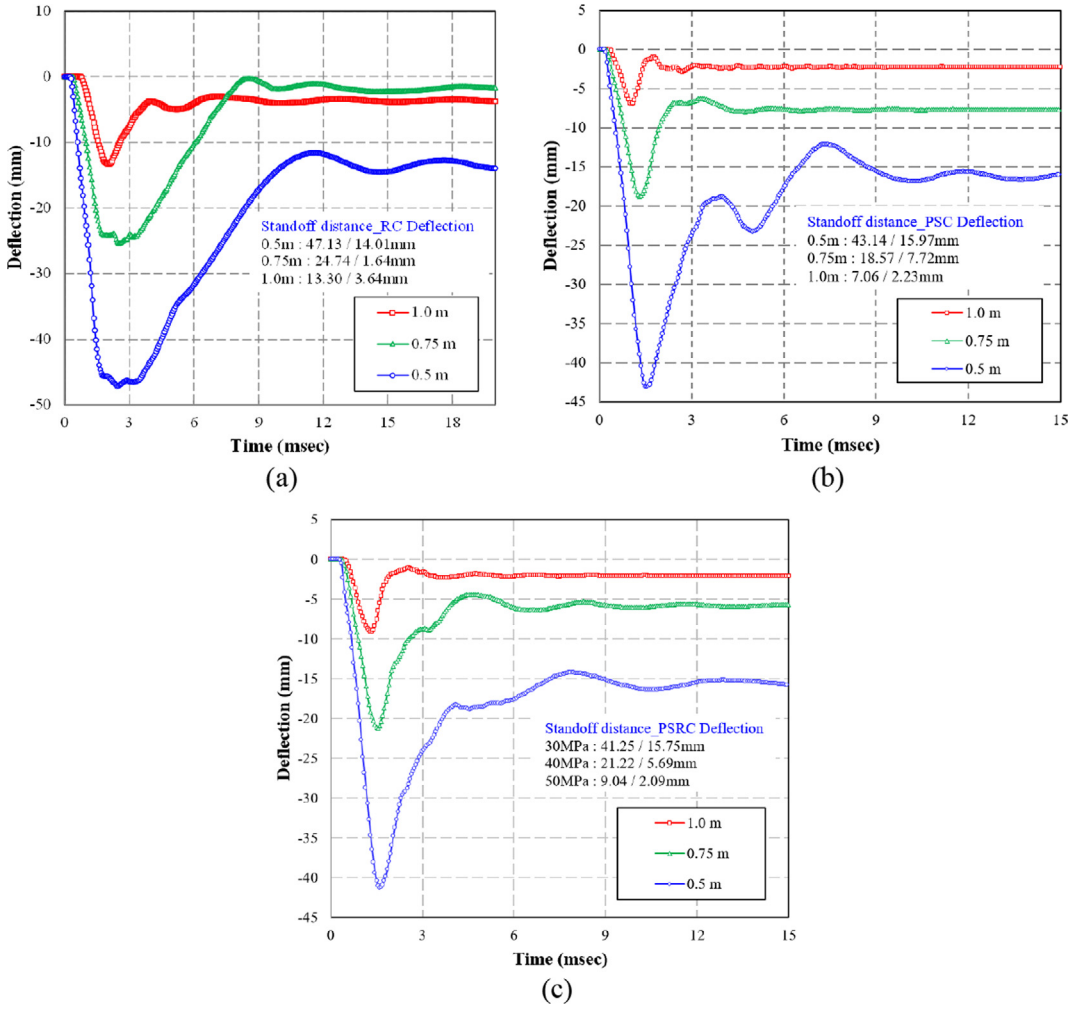


**Fig. 27.** Time-deflection curves according to standoff distance: (a) RC specimen; (b) PSC specimen; (c) PSRC specimen.

## 6. Conclusions

To evaluate the blast behavior of bi-directional prestressed concrete and reinforced concrete panel under blast loading, blast tests were carried out on RC, PSC and PSRC panel specimens. The applied blast load was generated by detonating 25 kg ANFO explosive charge at 1.0 m standoff distance. The data acquisitions included blast waves of incident and reflected pressure, deflection, strains, PS forces, acceleration. Also, a precise finite element simulation model was calibrated and simulated to investigated evaluated blast resistance capacity and failure behavior as well as parametric effect. The following conclusions can be drawn from this study

1) The similarity between the results obtained by incident pressure measurement at 5 m distance from the blast test and calculated using ConWEP program proved that the accurate estimation of blast pressure load for protection design is possible.
2) PSC and PSRC specimens showed better shear resistance due to their higher structural rigidity than RC specimen. Unlike in the RC specimen, PSC and PSRC specimens had macro cracks along the shorter dimensional direction where compressive force was generated. Also, fewer flexural and shear macro cracks were generated in PSC and PSRC specimens than in the RC specimens from the blast test.
3) PSRC specimens had significantly better blast than RC and PSC members due to the improved structural stiffness and energy absorption capacity from PS tendons and steel rebars, respectively.
4) Although PSRC specimen had larger maximum deflection than PSC specimen, the blast resistance of PSRC specimen was better than PSC specimen. Therefore, blast performance and resistance evaluations on structures should be conducted using all behavioral data such as maximum and residual deflections, crack and failure patterns, energy absorption, damaged area, spalling depth, residual load carrying capacity, etc.
5) Using the experimental data, HFPB simulation FE program is calibrated to be used for parametric simulation study of the panel specimens using concrete strength and blast standoff distance variations. The simulation results were accurate and logical for RC, PSC, and PSRC panel members.
6) The simulation results showed that as the concrete compressive strength increased the blast resistance to explosive load improved. Also, the damage from the explosion becomes more serious as the standoff distance becomes closer. The PSRC specimen is better than RC and PSC specimens in the blast resistance against extreme loading, due to the loss of prestressing force from impulse effect on tendons and the presence of rebar.
7) The parametric simulations verified that damage assessment to concrete structures can be precisely performed on concrete members for various blast load type, structural condition, material types, etc.

## Conflicts of Interest

The authors declare no conflict of interest.

## Acknowledgements

This work was conducted using financial supports from the Nuclear Safety Research Program through the Korea Foundation of Nuclear Safety (KOFONS) under a financial resource from the Nuclear Safety and Security Commission (NSSC) of Republic of Korea (Grant no. 1403010) and National Research Foundation of Korea (NRF) grant funded by the Korea government (MSIT, Grant no. 2016R1A2B3009444).

## References

[1] http://www.tiic.go.kr, NIS (National Intelligence Services), Terrorism Information Integration Center, 2009.
[2] W.E. Baker, Explosions in Air, Wilfred Baker Engineering, San Antonio, 1973.
[3] D.W. Hyde, Fundamental of Protective Design for Conventional Weapons. Conventional Weapons Effects (TM5-8511-1). United States Army Waterway Experiment Station. Vicksburg, Miss, 1992.
[4] Theodor Krauthammer, Blast-Resistant Structural Concrete and Steel Connections, Int. J. Impact Eng. 22 (9) (1999) 887–910.
[5] D. Karagiozova, G.N. Nurick, G.S. Langdon, Behavior of sandwich panels subject to intense air blast – part 2: numerical simulation, Compos. Struct. 91 (4) (2009) 442–450.
[6] S.W. Lee, S.J. Choi, J.H.J. Kim, Analytical study of failure damage to 270,000-kL LNG storage tank under blast loading, Comput. Concr. 17 (2) (2016) 201–214.
[7] Y. Xia, C. Wu, Z.X. Liu, Y. Yuan, Protective effect of graded density aluminium foam on RC slab under blast loading-An experimental study, Constr. Build. Mater. 111 (2016) 209–222.
[8] L. Mao, S.J. Barnett, A. Tyas, J. Warren, G.K. Schleyer, S.S. Zaini, Response of small scale ultra high performance fibre reinforced concrete slabs to blast loading, Constr. Build. Mater. 93 (2015) 822–830.
[9] S. Lan, T.S. Lok, L. Heng, Composite structural panels subjected to explosive loading, Constr. Build. Mater. 19 (5) (2005) 387–395.
[10] M. Foglar, R. Hajek, J. Fladr, J. Pachman, J. Stoller, Full-scale experimental testing of the blast resistance of HPFRC and UHPFRC bridge decks, Constr. Build. Mater. 145 (2017) 588–601.
[11] C.A. Ross, M.R. Purcell, E.L. Jerome, Blast response of concrete beams and slabs externally reinforced with fibre reinforced plastics (FRP), in: Proceedings of the structure. Congress. XV-building to last, Portland, USA, 1997: 673–677.
[12] L.C. Muszynski, M.R. Purcell, Use of composite reinforcement to strengthen concrete and air-enterained concrete masonry walls against air blast, J. Compos. Constr. 7 (2) (2003) 98–108.
[13] K.B. Morrill, L.J. Malvar, J.E. Crawford, J.M. Ferritto. Blast resistance design and retrofit of reinforced concrete columns and walls, in: Securing the Future Proceedings of Structures Congress, Nashville, Tennessee, USA, 2004.
[14] J.S. Davidson, J.R. Porter, R.J. Dinan, M.I. Hammons, J.D. Connell, Explosive testing of polymer retrofit masonry walls, J. Perform. Constr. Facil 18 (2) (2004) 100–106.
[15] M.G. Oesterle, Blast Simulator Wall Tests: Experimental Methods and Mitigation Strategies for Reinforced Concrete and Concrete Masonry (Doctoral Thesis), University of California, San Diego, USA, 2009.
[16] J.H. Ha, N.H. Yi, S.B. Kim, J.K. Choi, J.H.J. Kim, Experimental study on blast resistance improvement of RC panels by FRP retrofitting, J. Korea Concr. Inst. (Korean). 22 (1) (2010) 93–102.
[17] J.H. Ha, N.H. Yi, J.K. Choi, J.H.J. Kim, Experimental study on hybrid CFRP-PU strengthening effect on RC panels under blast loading, Compos. Struct. 93 (8) (2011) 2070–2082.
[18] N.H. Yi, J.H.J. Kim, T.S. Han, Y.G. Cho, J.H. Lee, Blast-resistant characteristics of ultra-high strength concrete and reactive powder concrete, Constr. Build. Mater. 28 (1) (2011) 694–707.
[19] N.H. Yi, S.W. Lee, J.W. Kim, J.H.J. Kim, Impact-resistant capacity and failure behavior of unbonded bi-directional PSC panels, Int. J. Impact Eng. 72 (2014) 40–55.
[20] N.H. Yi, S.J. Choi, S.W. Lee, J.H.J. Kim, Failure behavior of unbonded bi-directional prestressed concrete panels under RABT fire loading, Fire Saf. J. 71 (2015) 123–133.
[21] KINS/AR-897. Korea Institute of Nuclear Safety. Singori Unit 1 Operating Permit Screening and Safety Tests, 2010.
[22] S.J. Choi, S.W. Lee, J.H.J. Kim, Impact or blast induced fire simulation of bi-directional PSC panel considering concrete confinement and spalling effect, Eng. Struct. (2017).
[23] Sofinel. Reactor Building Containment Structural Design Criteria. Framatome-Korea Electric Co. Technical Specification, 1984:9441.
[24] TM5-1300/AFR 88-2/NAVFAC P-39. Structures to Resist the Effects of Accidental Explosions. Joint Departments of the Army, Air Force and Navy. Washington DC, 1990.
[25] TM5-855-1/AFPAM32-1147/NAVFACP-1080/DAHSCWEMAN-97. Design and Analysis of Hardened Structures to Conventional Weapons Effects. Joint Departments of the Army, Air Force, Navy and the Defense Special Weapons Agency. Washington DC; 1997.
[26] NP-3774, Construction Technology Laboratories. Concrete Containment Structural Element Tests: Half-Thickness Element Tests-Description and Results. Electric Power Research Institute. Illinois, 1984.
[27] NP-3774, Construction Technology Laboratories, Concrete Containment Structural Element Tests: Half-Thickness Element Tests-Detailed Test Data. Electric Power Research Institute. Illinois, 1984.
[28] H.J. Kim, Blast Analysis of FRP-Retrofitted Concrete Structures Considering FRP Failure Mechanisms (Ph.D Thesis), Yonsei University, 2007.

[29] L.J. Malvar, J.E. Crawford, J.W. Wesevich, D. Simons, A Plasticity concrete material model for DYNA3D, Int. J. Impact Eng. 19 (9/10) (1997) 847–873.
[30] H.C. Fu, M.A. Erki, M. Seckin, Review of effects of loading rate on reinforced concrete, J. Struct. Eng. 117 (12) (1991) 3660–3679.
[31] B.P. Hughes, R. Gregory, Concrete subjected to high rates of loading in compression, Mag. Concr. Res. 24 (78) (1972) 25–36.
[32] S.A. Kaplan, Factors affecting the relationship between rate of loading and measured compressive strength of concrete, Mag. Concr. Res. 32 (111) (1980) 79–88.
[33] T. Tang, L.E. Malvern, D.A. Jenkins, Rate effects in uniaxial dynamic compression of concrete, J. Eng. Mech. 118 (1) (1992) 108–124.
[34] M.S. Williams, Modeling of local impact effects on plain and reinforced concrete, Struct. J. 91 (2) (1994) 178–187.
[35] J. Halquist, LS-DYNA keyword user's manual version 971, Livermore Software Technology Corporation, Livermore, CA, 2007.
[36] Kai Xu, Lu. Yong, Numerical simulation study of spallation in reinforced concrete plates subjected to blast loading, Comput. Struct. 84 (5) (2006) 431–438.
[37] H. Jiang, M.G. Chorzepa, An effective numerical simulation methodology to predict the impact response of pre-stressed concrete members, Eng. Fail. Anal. 55 (2015) 63–78.